UC San Diego

UC San Diego Electronic Theses and Dissertations

Title

The magnetic characterization of metal-doped synthetic melanin nanomaterials

Permalink

https://escholarship.org/uc/item/3049q3vq

Author

Cay, Kristine Samantha

Publication Date

2020

Peer reviewed|Thesis/dissertation

eScholarship.org Powered by the California Digital Library
University of California

UNIVERSITY OF CALIFORNIA SAN DIEGO

The magnetic characterization of metal-doped synthetic melanin nanomaterials

A thesis submitted in partial satisfaction of the requirements
for the degree Master of Science

in

Chemistry

by

Kristine S. Cay

Committee in charge:

Professor Jeffrey D. Rinehart, Chair
Professor Stacey Brydges
Professor Alina Schimpf

2020

The thesis of Kristine S. Cay is approved, and it is acceptable in quality and form for publication on microfilm and electronically:

Chair

University of California San Diego

2020

DEDICATION

This manual and the work described herein

are dedicated to

Zarah Hazel Cay

in loving memory.

VII.XIX.MCMLXXXIX

EPIGRAPH

All my life through,
the new sights of Nature
made me rejoice like a child.

Marie Curie

TABLE OF CONTENTS

LIST OF ABBREVIATIONS

1,8-DHN	=	1,8-Dihydroxynaphthalene
2SCD	=	2-*S*-Cysteinyldopa
5SCD	=	5-*S*-Cysteinyldopa
AFM	=	Atomic Force Microscopy
AqpZ	=	AquaporinZ
ATR-IR	=	Attenuated total reflectance infrared
CNT	=	Carbon nanotube
CP	=	Cross-polarization
CPPI	=	Cross-polarization polarization-inversion
DA	=	Dopamine
DA·HCl	=	Dopamine Hydrochloride
DAQ	=	Dopaminequinone
D-clay	=	PDA-modified clay hydrogel
DHI	=	5,6-Dihydroxyindole
DHICA	=	5,6-Dihydroxyindole-2-carboxylic acid
DLS	=	Dynamic Light Scattering
DMAET	=	Dimethylaminoethanethiol
Dopa	=	3,4-dihydroxyphenylalanine
DQ	=	Dopaquinone
emu	=	Electromagnetic unit
EPR	=	Electron paramagnetic resonance
ES-HRMS	=	Electrospray ionization high-resolution mass spectrometry

Fe-BTC	=	Iron(III)-1,3,5-benzenetricarboxylate
Fe-PDA	=	Iron-doped polydopamine
GO	=	Graphene oxide
GOD	=	Glucose oxidase
HPLC-MS	=	High-performance liquid chromatography mass spectrometry
h.s.	=	High spin
ICP-MS	=	Inductively-Coupled Plasma Mass Spectrometry
LIB	=	Lithium ion battery
l.s.	=	Low spin
MALDI-MS	=	Matrix-assisted laser desorption/ionization–mass spectrometry
MAP	=	Mussel adhesive protein
MAS	=	Magic angle spinning
MPD	=	*m*-phenylenediamine
MOF	=	Metal organic framework
MRI	=	Magnetic resonance imaging
NPs	=	Nanoparticles
O_h	=	Octahedral
PA	=	Photoacoustic
PBS	=	Phosphate buffered saline
PDA	=	Polydopamine
PE	=	Polyethylene
PEG	=	Polyethylene glycol
PET/CT	=	Positron emission tomography-computed tomography

PFC	=	Perfluorocarbon
PLA	=	Polylactic acid
ppb	=	parts per billion
PSf	=	Polysufone
PXRD	=	Powder X-ray diffraction
Rh6G	=	Rhodamine 6G
SANS	=	Small-angle neutron scattering
SEI	=	Solid-electrolyte-interphase
SEM	=	Scanning Electron Microscopy
SMFS	=	Single molecule force spectroscopy
Smolecule	=	Small-molecule
ssNMR	=	Solid state nuclear magnetic resonance
SQUID	=	Superconducting Quantum Interference Device
TEM	=	Transmission Electron Microscopy
TMC	=	Trimesoyl chloride
TME	=	Tumor microenvironment
Tris	=	Tris(hydroxymethyl)aminomethane
Tyrp1	=	DHICA oxidase
Tyrp2	=	Dopachrome tautomerase
UV	=	Ultraviolet
XPS	=	X-ray photoelectron spectroscopy

LIST OF SYMBOLS

Å	=	Ångström
β	=	Bohr magneton
D	=	Anisotropy term
δ	=	Chemical shift
g	=	Gyromagnetic value
H	=	Magnetic field
$\widehat{H}$	=	Heisenberg-Dirac-Van-Vleck (HDVV) Hamiltonian operator
J	=	Magnetic coupling constant
K	=	Kelvin
k	=	Boltzmann constant
M	=	Molar
μ_B	=	Bohr magneton unit
N	=	Avogadro's number
S	=	Spin
$\hat{S}_1$	=	Spin operator
T	=	Temperature
χ	=	Magnetic susceptibility
$\chi_M T$	=	Product of molar magnetic susceptibility and temperature

LIST OF FIGURES

LIST OF SCHEMA

LIST OF TABLES

ACKNOWLEDGMENTS

Over the course of my Master's program, I established the following mantra: "Stay hydrated, keep the hype alive, and edify your village", and so it is only fitting to take this opportunity to express my deepest gratitude for the village who worked so tirelessly to edify and encourage me, hype me up, and remind me to stay hydrated throughout my scientific endeavors.

I am grateful for my advisor and mentor, Prof. Jeffrey Rinehart, for his informed guidance and unfailing support of me. There are no words which can adequately express the profound gratitude I have for his patience with and acceptance of me, especially when I felt unfit to join a field such as this. I am thankful for all the conversations which pushed the boundaries of my knowledge and broadened the scope of my thinking. I am thankful for his encouragement of creativity when approaching problems and brainstorming solutions. And I am immensely grateful for his unwavering faith in me, without which I would likely not have remained where I am now.

I would like to thank the members of my committee, Prof. Stacey Brydges and Prof. Alina Schimpf, for their support in my endeavors and for always reminding me that I am welcome here and that I have a place in the scientific community.

Much appreciation goes to the members of the Rinehart group, especially Phil Bunting and Max Bernbeck for their mentorship in magnetism, and Tara Zand, for our countless conversations about polydopamine. Special thanks go to Hayley Fong, who has worked tirelessly in collaboration with me on this project.

I would like to thank Mason Mackey from the National Center for Microscopy and Imaging Research (NCMIR) for his expertise in TEM imaging, as well as Dr. Ryan Nicholl from the Nano3 facility of Qualcomm Institute for his guidance in SEM imaging. Additionally, I am thankful for Dr. Neal Arakawa for this assistance with ICP-MS characterization and analysis.

Many thanks go to Dr. Robert Ternansky for his unfailing support of me not only as a student, but also as an educator. It has been an incredible honor to learn from him. I would like to thank Dr. Regis Komperda and Dr. Carly Schnoebelen for the many wonderful conversations we have had regarding chemical education and for their support in my teaching endeavors. And I would like to thank Mrs. Sharon Veenhof, my high school Advanced Placement chemistry teacher, for her exemplary teaching and for demonstrating the type of educator I aspire to be.

Incredibly special thanks go to Dr. Katherine Hatcher and Claire Costenoble-Caherty, for holding me accountable for the production of this manual, especially in light of the COVID-19 global pandemic and amidst the events of social and political unrest. Their support and (virtual) company has been monumental throughout this writing process.

I am exceptionally grateful for the conductors of the #HypeTrain, Dr. César Urbana-Blanco, Dr. Michelle Muzzio, Dr. Fiona Kearns, Safia Jilani, and Stanna Dorn, for their hype for and encouragement of me, as well as countless other, throughout my scientific journey. I would also like to thank Dr. Jen Heemstra for her mentorship and friendship in throughout this voyage.

Many thanks go to my closest friends: Gerick Yabut and Danielle Seckler, for their support of me through high school, into university, and throughout graduate school; Taylor Wyrick, for all of her support, hype, and all the late night coffee shop study sessions; Haley Palm and Alysia Kohlbrand, for their support through graduate school; Dr. John Kim for his support, guidance and friendship; and Shayna Holness and Dr. Pauline Olsen, for their endless support. And for their constant reminders to drink water. I would like to thank Dr. Jessie Moreton for her friendship and for her guidance in navigating the field of science whilst also embracing and celebrating the social aspects which make me unique.

I would like to express my deepest gratitude for my mentor, close friend, the big brother I never had, Alex Mantanona. For always being there, in the highlands and in the heartache. For his guidance in professional and personal matters. For his unrelenting and unwavering support. For his patience with me and gentleness toward me. For speaking with grace and with truth. For keeping me grounded and for compassionately reasoning with me when I have been nonsensical. For meeting me where I was and providing me the space to grow, to learn, to explore. Senpai, there are no words in my expansive vocabulary that will ever adequately describe how thankful I am for you. But I will start with two: thank you.

To my closest friend, my sweetest sister, Ashley "Nubbsie" Pineda: thank you. Thank you for walking alongside me throughout it all. Thank you sharing in my greatest joys and deepest sorrows. Thank you for caring for me when I could not do it myself. Thank you for teaching me patience by being patient with me yourself. Thank you for fiercely protecting me and for reminding me of where I was and how far I have come. You are the glitter in this pile of bricks and the one who reminds me to gaze at the clouds when I have been too busy with my head in the ground. Thank you for being my home. Thank you for being my safe space. Thank you for being in my corner.

And finally, all my thanks go to my mama. For her unwavering confidence in me. For her unrelenting support of me. For being my rock and my stronghold. For telling me to keep the faith. And for always reminding me to be inspired and be an inspiration. Thank you.

This thesis is co-authored with Cay, Kristine S., Fong, Hayley A. and Rinehart, Jeffrey D. The thesis author was the primary author of this work.

VITA

2014-2018 Bachelor of Science, University of California San Diego

2018-2020 Teaching Assistant, University of California San Diego

2018-2020 Master of Science, University of California San Diego

PUBLICATIONS

1. Mantanona, A. J.; Tolentino, D. R.; **Cay, K. S.**; Gemicky, M.; Jazzar, R.; Bertrand, G.; Rinehart, J. D., "Tuning electronic Structure through halide modulation of mesoionic carbene cobalt complexes." *Dalton Trans.*, **2020**, *49*, 2426-2430.
2. Xie, Y.; Krug, K.; **Cay, K. S.**; Kalaj, M.; Collin-McCallum, N.; Siwicka, Z.; Wang, Z.; Gianneschi, N.; Burkart, M.; Rinehart, J. D. "Peroxidase-like reactivity at iron-chelation sites in a mesoporous synthetic melanin." *Chin. Chem. Soc.* **2020** (under review).

FIELDS OF STUDY

Major Field: Chemistry

Studies in Inorganic and Magnetochemistry
Professor Jeffrey D. Rinehart

ABSTRACT OF THE THESIS

The magnetic characterization of metal-doped synthetic melanin nanomaterials

by

Kristine S. Cay

Master of Science in Chemistry

University of California San Diego, 2020

Professor Jeffrey D. Rinehart, Chair

Synthetic melanins are incredibly versatile materials that have captured the attention of chemists and materials scientists due to the remarkable properties they share with natural melanins, such as adhesion, sequestration of metals and organic molecules, and biocompatibility. The facile and sustainable production of these materials involves oxidation of the catechol moiety of the dopamine monomer in mild and alkaline conditions, inducing the polymerization of the starting material into polydopamine. These materials have myriad applications, in areas such as energy

(e.g. lithium ion batteries, supercapacitors), water treatment (e.g. metal and organic pollutant removal, desalination), and biomedical sciences (e.g. drug delivery, imaging contrast agents). The structure and function of these polydopamine materials is discussed in further detail in Chapter 1. Chapter 2 describes the materials and methods used to prepare synthetic melanins for characterization *via* magnetometry to probe the effects of small variations employed in the synthetic procedures on the electronic structure of these materials. In Chapter 3, the results of this work are discussed, showing evidence of the buffer solution's influence on the magnetic behavior of the samples. Finally, Chapter 4 proposes future studies for the continuation of this project.

CHAPTER 1: INTRODUCTION TO SYNTHETIC MELANIN MATERIALS

1.1 Introduction to Melanin and its Synthetic Analogues

Melanin is a broad term used to describe a ubiquitous, poorly defined, dark biopolymeric pigment that is produced in melanocytes, adipocytes, neurons, and in the pigmented epithelium of eye retina.[1] Melanins are responsible for color in living cells as well as protective properties against ultraviolet (UV) radiation and is generally biosynthesized through the enzymatic oxidation of L-tyrosine by tyrosinase, exhibiting a broad variety of properties, including light absorbance, reductive-oxidative properties, and metal chelation.[2,3] In humans in three forms: (i) brown-black eumelanin, (ii) yellow to reddish-brown pheomelanin, and (iii) neuromelanin.[4] Whereas eumelanins are derived from 5,6-dihydrxyindoles (DHI), pheomelanins are biosynthesized through the involvement of cysteine residues in the enzymatic oxidation of tyrosine, forming cysteinyldopas, and neuromelanin, found in the *subsantia nigra* of the brain, is derived from dopamine moieties.[5,6]

Despite extensive study of this pigment, with the discovery of melanocytes in the mid-twentieth century and studies of human pigmentation disorders dating as early as ca. 2200 B.C.E, the exact structure of melanin, the organization of its constituent molecules, and the mechanism by which the polymerization occurs have yet to be unambiguously determined.[4,7] Several factors contribute to the challenge of isolation and characterization of natural melanins. For example, melanins are not indefinitely stable and may undergo structural degradation given prolonged storage to certain chemical conditions (e.g. acidic, alkaline, oxygenated, peroxidic), or may suffer alterations due to exposure to elevated temperatures or light. Moreover, the difficulty in isolating this pigment can be dependent on its source. To give an example, sepia melanin, or sepia ink, is

one of the most accessible sources of eumelanin and can be isolated by centrifugation and storage in dilute acid at 4°C. In contrast, the isolation and purification of human neuromelanin is extraordinarily complex, as the pigment is securely retained within the tissue matrix in the brain and contains several impurities, such as glycolipids, chelated metals, and proteins, further complicating the purification process.[8]

To address challenges in characterizing natural melanin, recent progress has been made in the design and characterization of synthetic melanin mimics. The most common of these is polydopamine (PDA), a material that has been widely investigated and for which over twenty thousand studies have been published since 2007.[4,9,10] PDA is a black amorphous polymer that can be synthesized through aerobic autoxidation of a catecholamine, typically dopamine (DA), although other analogues have incorporated L-3,4-dihydroxyphenylalanine (L-DOPA) as the starting monomer, in alkaline conditions, however a variety of other starting monomers have been found in the polymer (Scheme 1.1).[9,11]

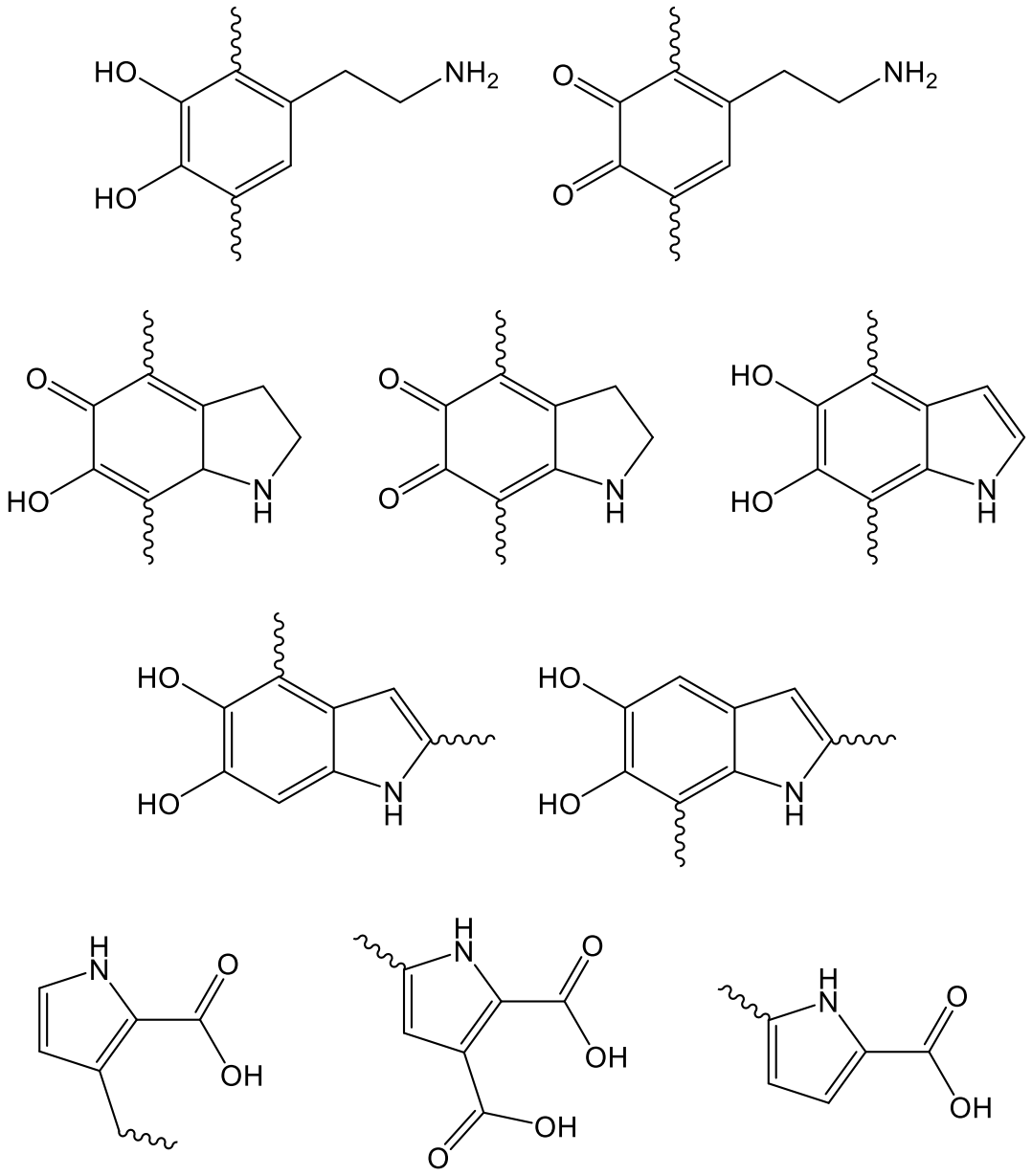

Scheme 1.1. Polymerization sites of monomer units found in PDA. (Adapted with permission from Reference 9. Copyright 2019 John Wiley & Sons, Inc.).

As shown in Scheme 1.1, the monomer moieties ostensibly polymerize in a variety of positions, demonstrating the complexity of characterizing the material. Since the structure of PDA is largely dependent on the means of preparation and the morphology of the material (i.e. film coating, nanoparticulate, aggregated material), the analytical results and structural characterization of different samples should be carefully compared.[9]

1.1.1 Structural Characterization

It has been previously proposed that eumelanin is comprised of a mixture of covalent polymers (C–C bonding) and non-covalent aggregates, which stack through π–π and hydrogen-bonding interactions. Drawing from these propositions, several analytical methods have been applied in an attempt to elucidate the general structure of PDA.[12] Until recently, two structural models were prominently assumed: the "open-chain polycatechol/quinone" model, where linear sequences of catecholamine units were covalently linked through biphenyl-type bonds, and the "eumelanin" model, in which 5,6-dihydroxyindole (DHI) moieties polymerized through the cyclization and linking of dopaminequinone.[13,14] However, further examination of the literature suggests that PDA polymerizes in a similar fashion to hydroquinone or catechol moieties.[16-18]

In 2012, a study by Dreyer *et al.* proposed a new structural model of PDA. Using solid state nuclear magnetic resonance (ssNMR) spectroscopy to analyze a dried solid sample, the ^{15}N-NMR spectrum revealed a chemical shift (δ) near –260 ppm, implying the presence of a nitrogen heterocycle, such as an indole or indoline moiety. These have been proposed to be involved in the structural composition of many eumelanins. The higher chemical shifts PDA-based peaks and the absence of signals indicative the presence of a primary amine, the authors concluded that the dopamine starting material underwent cyclization and that the tris(hydroxymethyl)aminomethane (Tris) buffer did not incorporate into the structure of the polymer to a significant extent. Studies using ^{13}C-NMR exhibited a pair of chemical signals spanning from δ = 110 ppm to δ = 150 ppm, which were also present in the solution state spectrum of the dopamine moiety, confirming that the aromatic ring of the molecule was retained. Furthermore, a shift observed at δ = 173 ppm showed that the catechol group of the dopamine starting material underwent partial or complete oxidation to the semi- and *ortho*-quinones, respectively. Chemical shifts between δ = 30 ppm to δ

= 70 ppm are also, characteristic of saturated aliphatic carbons, further corroborating the formation of an indoline product. Absence of any peaks indicating the presence of unsaturated olefins confirmed that no indole species had been produced. Powder X-ray diffraction (PXRD) was then performed to determine the presence of extended π–π stacking interactions. The findings of these analyses indicated that the monomers stacked with a 3.8 Ångström (Å) *d*-spacing, consistent with other materials exhibiting π-stacking, which, the authors suggest, either facilitate or are a result of charge transfer between the faces of the monomers. Their collective analyses propose that PDA is a supramolecular aggregate of monomers, as opposed to the previously proposed mixed model of covalent polymers and non-covalent aggregates.[12]

To further investigate the structure of PDA, Liebscher *et al*. used carbon-13 cross-polarization polarization-inversion magic angle spinning NMR (^{13}C CPPI MAS NMR), proton magic angle spinning NMR (^{1}H MAS NMR), electrospray ionization high-resolution mass spectrometry (ES-HRMS), X-ray photoelectron spectroscopy (XPS), and Fourier transform infrared (FTIR) spectroscopy in a 2013 study.[19] Samples were prepared using two previously reported methods, using either Tris buffer or phosphate buffer.[20] Their FTIR spectroscopic findings revealed no discrepancies between either sample. ^{1}H-NMR analysis revealed chemical shifts that were consistent with the existence of indole and 2,3-dihydroindole moieties within the polymer. Chemical shifts of δ = 30 ppm and δ = 40 ppm suggested the presence of aliphatic carbons that may be assigned to those in the five-membered ring of indole and indoline species, or to the noncyclized aminoethyl units in dopamine or *o*-quinone moieties. Additionally, spectra showed signals at δ = 145 and between δ = 170 – 180 ppm, characteristic of phenolic carbons and carbonyl carbons, respectively, suggesting the presence of a diketone, a diol, or a species containing both ketone and hydroxy functionalization. The possibility of monomers containing a saturated

bridgehead C–H carbon was eliminated for lack of a chemical shift around δ = 60 ppm. While all reported major signals were consistent with those of Dreyer's study, other features not previously reported were revealed in Liebscher's cross-polarization (CP) studies. Namely, chemical shifts at δ = 27 ppm and δ = 104 ppm were assigned to a benzylic CH_2 carbon and the C–H carbon at position 3 of the pyrrole ring in an indole moiety, respectively. The collective NMR analyses give rise to the proposed structure of PDA illustrated in Scheme 1.2.[19]

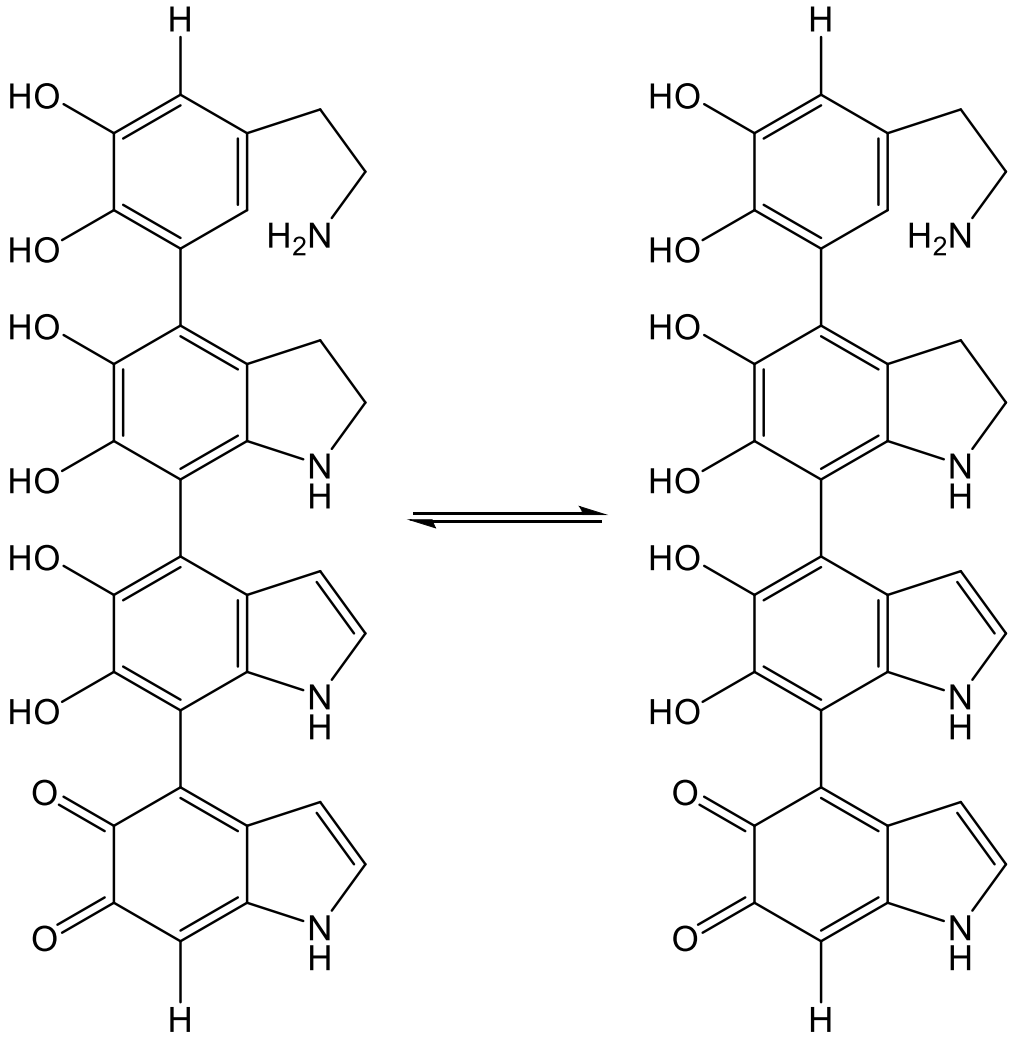

Scheme 1.2. Proposed structure of PDA. (Adapted with permission from Reference 19. Copyright 2013 American Chemical Society).

Results from MALDI-MS indicated the presence of open-chain dopamine units and suggests the existence of oligomers bearing different degrees of saturation, while finding from the

XPS experiments showed the absence of bands characteristic of imine nitrogens, as proposed by Shalev.[19,21] Given these results, several previously published hypotheses corroborate one another, while others were found to be contradictory.

In a 2014 study by Della Vecchia *et al*., it was found that Tris buffer was incorporated into the structure of the PDA polymer.[22] PDA samples were all prepared at pH = 8.5 with either phosphate, bicarbonate, or Tris buffers. To analyze each of the buffer's effects on the size of the nanoparticle, dynamic light scattering (DLS) measurements were taken for each sample. The findings of these experiments revealed that the extent of aggregation in the material is dependent on the DA concentration and monomers or small oligomers are added to the growing polymer chain with a low size dispersion during polymerization, while aggregation of larger oligomers occurred to a much lesser degree. Furthermore, average particle size appeared to be dependent on the buffer used in the preparation of the material, being larger when prepared with phosphate buffer, whilst particles prepared with Tris were markedly smaller. To examine the morphology of the nanoparticles, Small-Angle Neutron Scattering (SANS) studies were conducted. The results from these analyses suggested that while there appeared to be two-dimensional structures in the samples prepared with the phosphate and bicarbonate buffers, which is consistent with previous reports, the material prepared with Tris buffer appeared to have a three-dimensional fractal morphology. Electron Paramagnetic Resonance (EPR) experiments were then performed on dried samples to study the effects of both structural modification due to the buffer, as well as the aggregation mechanisms, on the paramagnetic centers of the polymer. From these studies, it was concluded that while signals attributed to carbon-centered radicals were predominant, the semi-quinone signal was also detected for all three cases and was particularly significant in the spectrum of the material prepared in Tris. The comprehensive results strongly support a monomer-polymer

growth regime, as opposed to a polymer-polymer growth regime, that can be tuned by varying experimental parameters. The model proposes rapid aggregation of small oligomer chains that arrange in distinct units which grow gradually in a comparatively homogenous manner, forming larger structures. [23]

A 2018 study by d'Ischia and colleagues utilised matrix-assisted laser desorption/ionization–mass spectrometry (MALDI-MS) to determine that PDA is structurally different from DHI-based melanins. Their studies exhibited that PDA is not comprised of moieties that are compatible with DHI-based oligomers which form the melanin biopolymer. Additional findings of this study concluded the PDA films were deposited with structural components that were unrelated to DHI oligomers or porphyrin-type tetramers, such as those found in melanin, using atomic force microscopy (AFM) and Raman spectroscopy.[24]

In 2019, Delsparastan *et al*. applied AFM-assisted single molecule force spectroscopy (SMFS) toward investigating the presence of significant polymeric fragments in the structure of polydopamine. PDA film samples were deposited onto Si_3N_4 AFM cantilevers. Their analyses indicated that their PDA film samples were comprised of high-molecular-weight polymer chains whose subunits were covalently bonded. While the results of this study confirmed the presence of polymers in the overall structure of PDA, it cannot be concluded that smaller oligomer components and small-molecule (smolecule) monomers are non-existent. Furthermore, it was found that PDA chains were associated by weak, reversible, and noncovalent interactions and that PDA chain growth occurs at the solid-liquid interface during the early stages of polymer synthesis. Collectively, these results agree with the notion that PDA is comprised of both covalent C–C bonds as well as non-covalent interactions amongst larger oligomer chains, contrasting the most common

hypothesis that PDA is a supramolecular aggregate of monomeric and/or oligomeric subunits held together by weak noncovalent interactions.[25]

In summary, much work has been done in attempt to uncover the perplexing structure of PDA, and while the results of some appear to corroborate those of previous studies, others seem to contradict one another. Although several structural properties of this material have been uncovered through various investigations, the exact structure of PDA has yet to be unambiguously determined and requires further examination.

1.1.2 Mechanistic Studies

While there has been much success in the development of synthetic melanins and materials with catechol functionalization, the structure of these polymers and the mechanisms by which they are formed are much less understood.[26] Several mechanisms have been proposed in a myriad of previous investigations, beginning with the study of the structure and polymerization of melanins. For example, it is known that eumelanin and pheomelanin are both derived from a common precursor, dopaquinone (DQ), which is formed through the oxidation of L-tyrosine by tyrosinase.[27] It had been speculated that 3,4-dihydroxyphenylalanine (Dopa) was precursor to DQ, until Cooksey *et al.* demonstrated that *o*-quinones are formed immediately in the beginning stages of melanogenesis.[28] The ethylamine of DQ undergoes cyclization to form cyclodopa, or leukodopachrome, which participates in a redox exchange with DQ, producing dopachrome, an orange-red intermediate, as well as.[29,30] The proposed biosynthetic pathway of the formation of eumelanin and pheomelanin are illustrated in Scheme 1.3.[27]

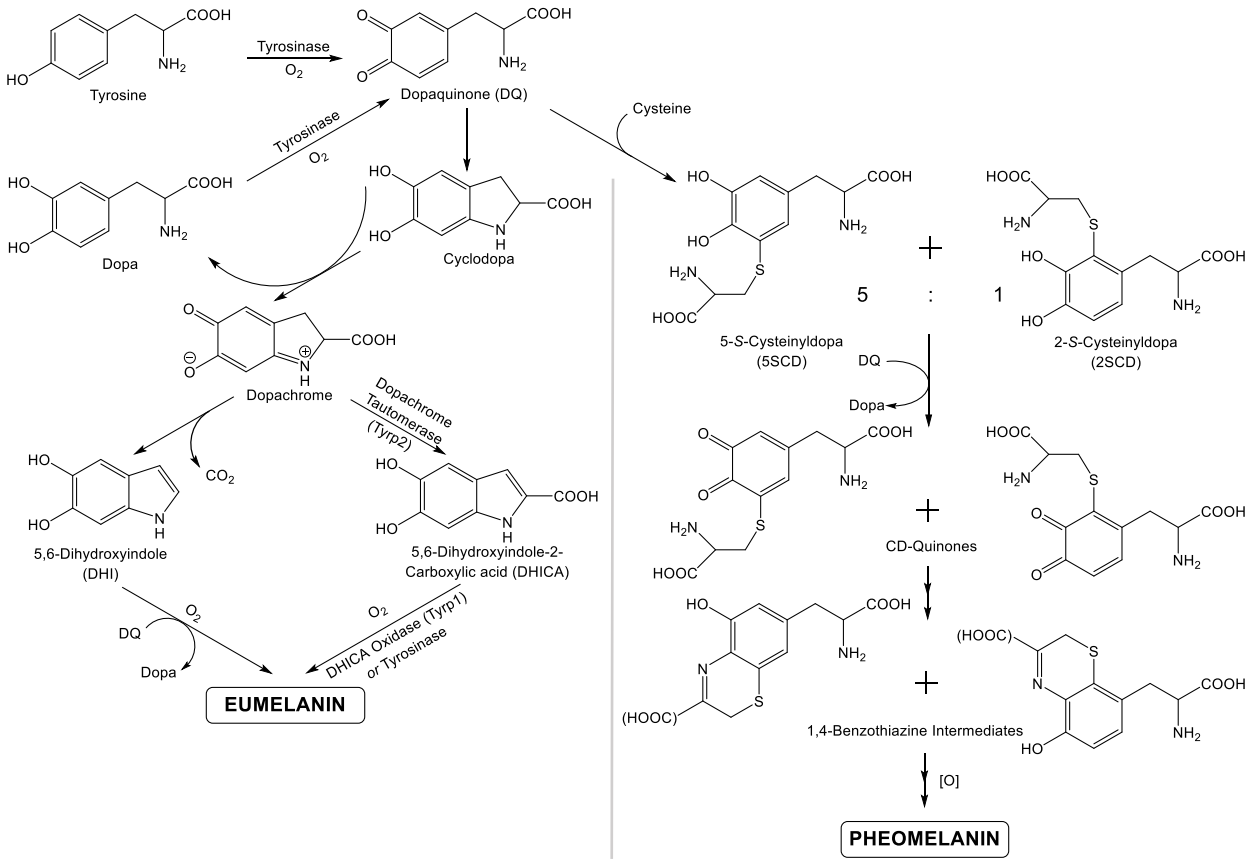

Scheme 1.3. Proposed model of the biosynthetic mechanisms leading to Eumelanin (left) and Pheomelanin (right). (Adapted with permission from Reference 27. Copyright 2019 John Wiley & Sons, Inc.).

The mechanism of eumelanin biosynthesis was derived from a postulation by Raper and Mason several decades before (Scheme 1.4).[29,30] Though Raper's study of the tyrosinase-tyrosine reaction puts forth several hypotheses for the pathway by which melanin is formed, there was much uncertainty surrounding the exact mechanism for the pigment's formation at the time of publication. For example, there was early debate whether the ethylamine cyclized at the 2- or 6-position; however, given extensive study of this material, it has been presently confirmed cyclization occurs at the 6-position.[31] It is worth noting that the melanin experimentally obtained from tyrosine *via* enzymatic oxidation by tyrosinase may not be identical to the pigment that is naturally produced in melanocytes, though it is likely that the former is an essential precursor in the production of natural melanin.[29] Scheme 1.4 illustrates the most probable currently proposed pathway for the biosynthesis of melanin.

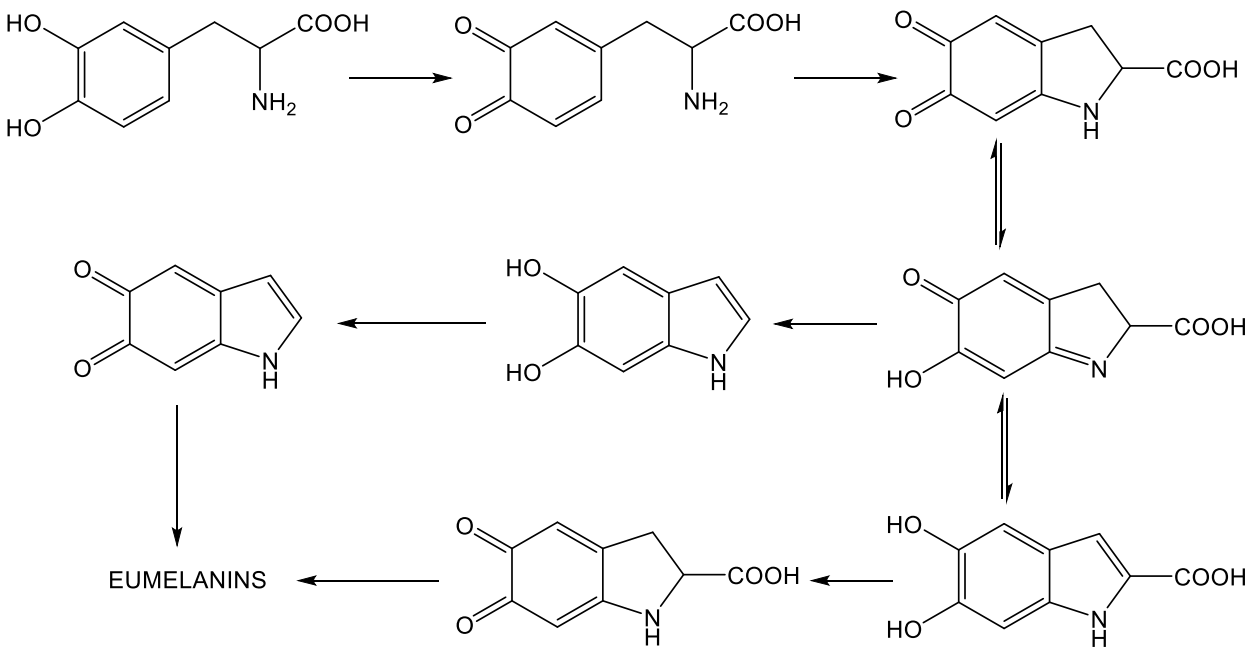

Scheme 1.4. Raper-Mason Scheme for the formation of eumelanins. (Adapted with permission from Reference 30. Copyright 2007 John Wiley & Sons, Inc.).

The Raper-Mason scheme implies that the polymerization of synthetic melanins proceeds primarily through the formation of covalent bonds. As discussed in Section 1.1.1, there exists a combination of both covalently bonded oligomers as well as non-covalently interacting oligomer chains. A 2012 study by Hong *et al*. revealed that a significant amount of dopamine remains unpolymerized to instead form a physical, self-assembled trimer of $(DA)_2$/DHI is present in PDA, which has been known to form *via* covalent polymerization, and is tightly enclosed within the polymer complex (Scheme 1.5). Remarkably, the previously proposed oxidative polymerization appears to occur simultaneously with the physical self-assembly of the trimer, indicating that polydopamine is produced through two distinct pathways. Additionally, it is speculated that the results of this study may likely be distinctive, as the PDA samples were prepared with phosphate buffered saline (PBS) solution, as opposed to the traditional use of Tris buffer. The formation of polydopamine in this study was monitored using High-Performance Liquid Chromatography Mass Spectrometry (HPLC-MS). Two elution peaks were detected, one at 5.0 minutes, indicative of the

presence of unpolymerized dopamine, and another at 14.4 minutes. Upon addition of the oxidizing agent sodium periodate, no shift in the elution times was observed, suggesting that the chemical structure of the eluate remained unchanged. Upon further spectrometric analysis, it was concluded that the compound that eluted at 14.4 minutes were physical assemblies of DA/DHI/Na^+, DA/DHI, and possibly $(DA)_2$/DHI. Investigations using ^{1}H-NMR provide evidence that an oxidative reaction occurs at the 2-position in DHI, resulting in the formation of a 2,2-linked DHI-DHI dimer, which can further react with dopamine to form a DA-DHI-DHI trimer. Polymer formation and intermolecular interactions that cause precipitation of the polymer were evaluated using a variety of computational methods, for which four models were devised: (i) a T-shaped interaction between a DA hydroxy hydrogen and the aromatic ring in DHI, in addition to hydrogen-bonding between a DHI hydroxy oxygen and a DA amino hydrogen; (ii) a cation-π interaction between a DA amine and a DHI aromatic ring, as well as hydrogen-bonding from the hydroxyl groups of each compound; (iii) a T-shaped interaction between a DA aromatic hydrogen and the aromatic ring in DHI, in addition to hydrogen-bonding between a DHI hydroxy oxygen and a DA amino hydrogen; and (iv) solely cation-π interactions, which appeared to be less stable than the other three models. Of the four models, the combination of the T-shape interaction and hydrogen-bonding seem to be most favorable.[32]

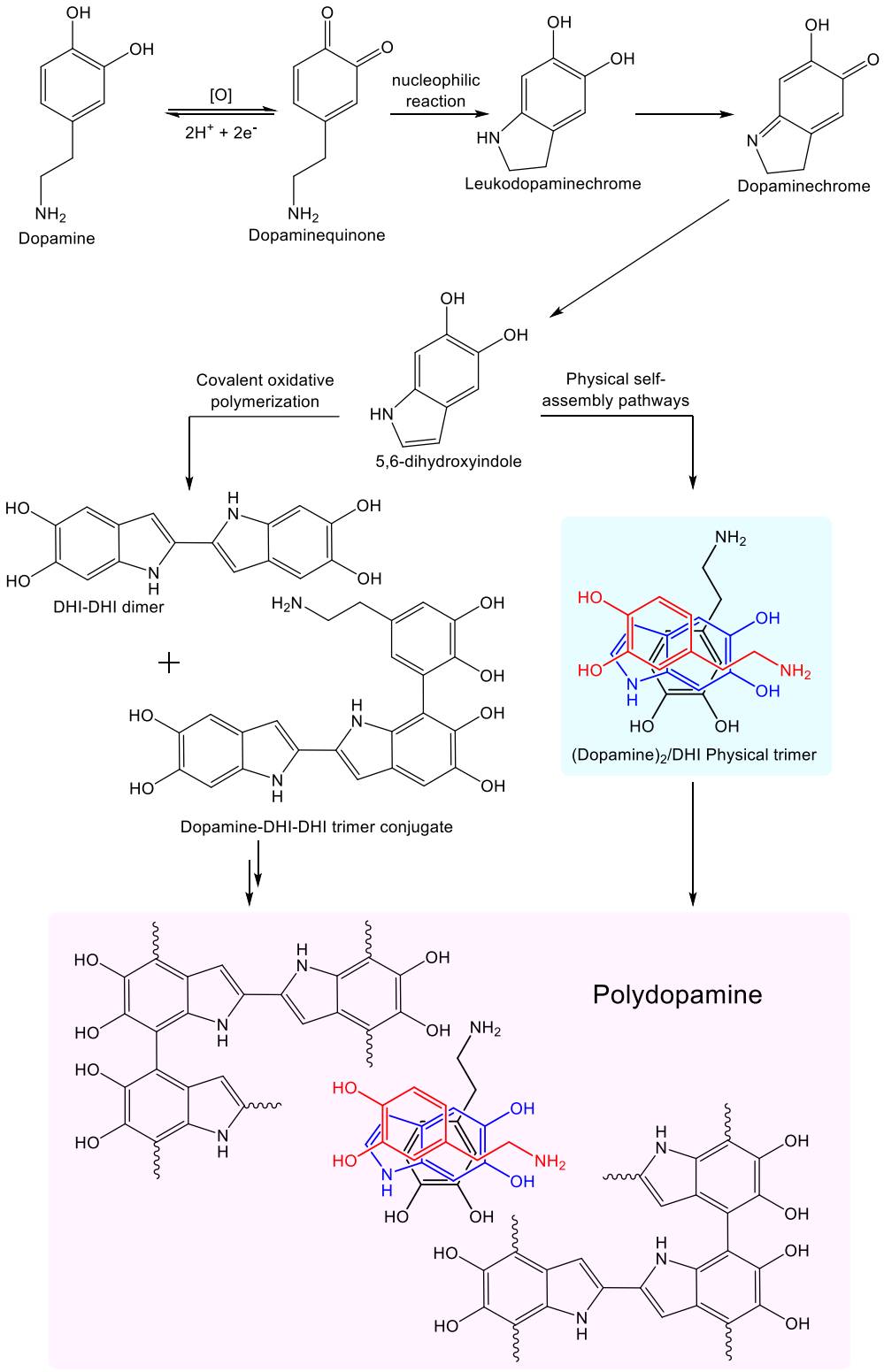

Scheme 1.5. Proposed mechanism of polydopamine *via* covalent oxidative polymerization and physical self-assembly of dopamine and DHI. (Adapted with permission from Reference 32. Copyright 2006 Springer Nature).

It had been previously discussed that Tris buffer, bearing an aliphatic primary amine, is incorporated into the structure of polydopamine.[22] The *o*-quinone of DQ or dopaminequinone (DAQ) can react with amines through three different pathways: (i) Michael addition, (ii) Schiff base formation, and (iii) Strecker degradation; thiols can also participate in Michael-type reactions with *o*-quinones but will not be discussed further here (Scheme 1.6).[26,33] Notably, aromatic amines tend to favor Michael additions whilst aliphatic amines are more selective toward Schiff base reactions and α-amino acids undergo Strecker degradations with *o*-quinones at high temperatures. Both Michael-addition and Schiff base formation pathways are strongly affected by pH. However, imine formation appears to be affected by chain length as well, where longer hydrocarbon chains reduce the basicity of the α-amine, enabling the formation of catechol-amine adducts at lower pH. Thus, it is reasonable that Tris buffer is incorporated into the structure of polydopamine *via* Schiff base formation due to its relatively high basicity (pH ≈ 9-11) despite its short, tri-substituted aliphatic branch.[26]

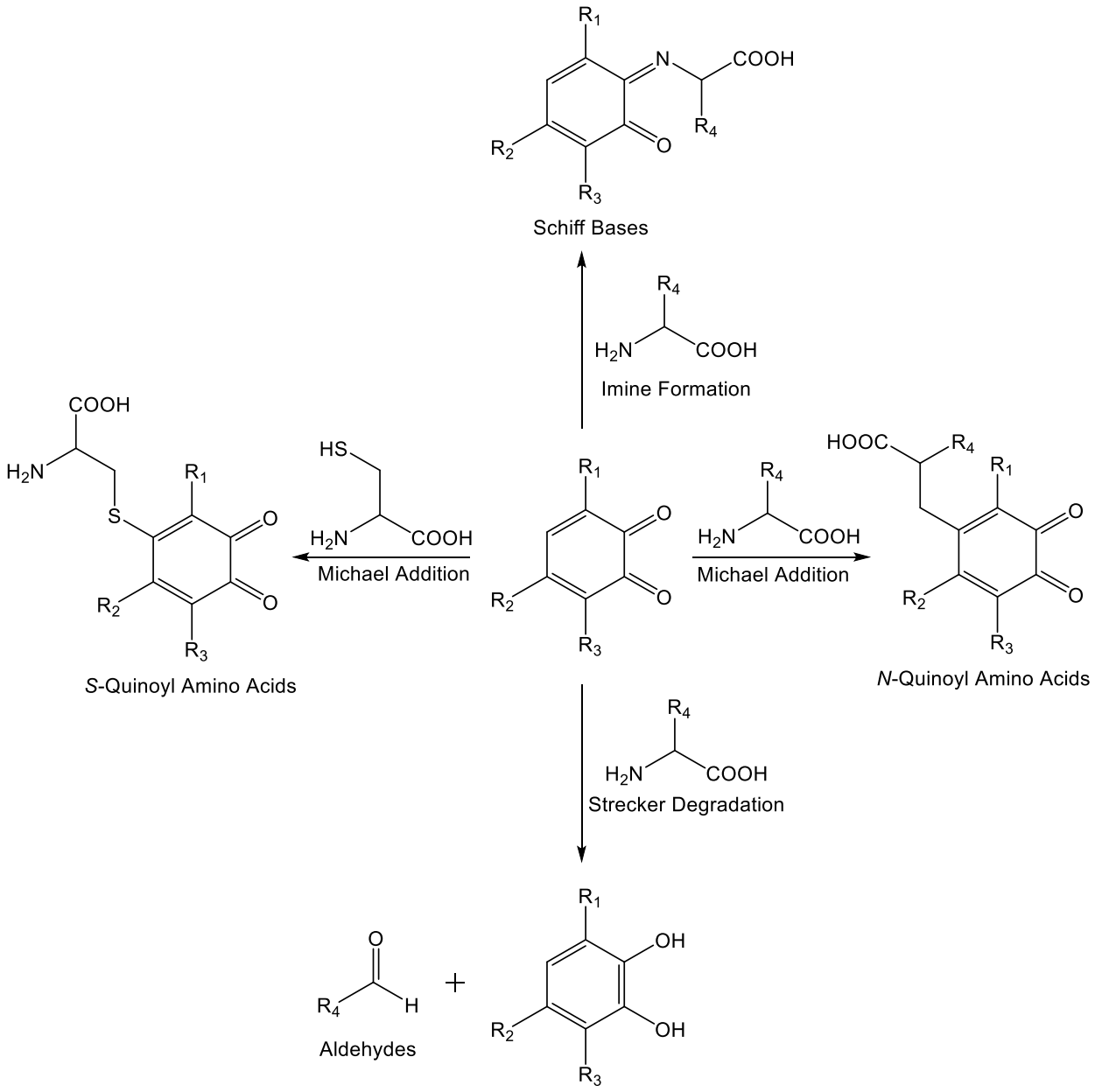

Scheme 1.6. Mechanisms for catechol reactivity with amines and thiols. (Adapted with permission from Reference 33. Copyright 2012 John Wiley & Sons, Inc.).

Moreover, the *o*-quinone polymer precursors can crosslink with each other *via* two pathways: (i) through a reverse dismutation pathway, in which highly reactive semi-quinone radicals are produced, forming di-dopa crosslinking upon further reaction, and (ii) through

tautomerization, in which α,β-dehydro derivatives are produced, also forming crosslinks upon further reaction (Scheme 1.7).[26,34,35]

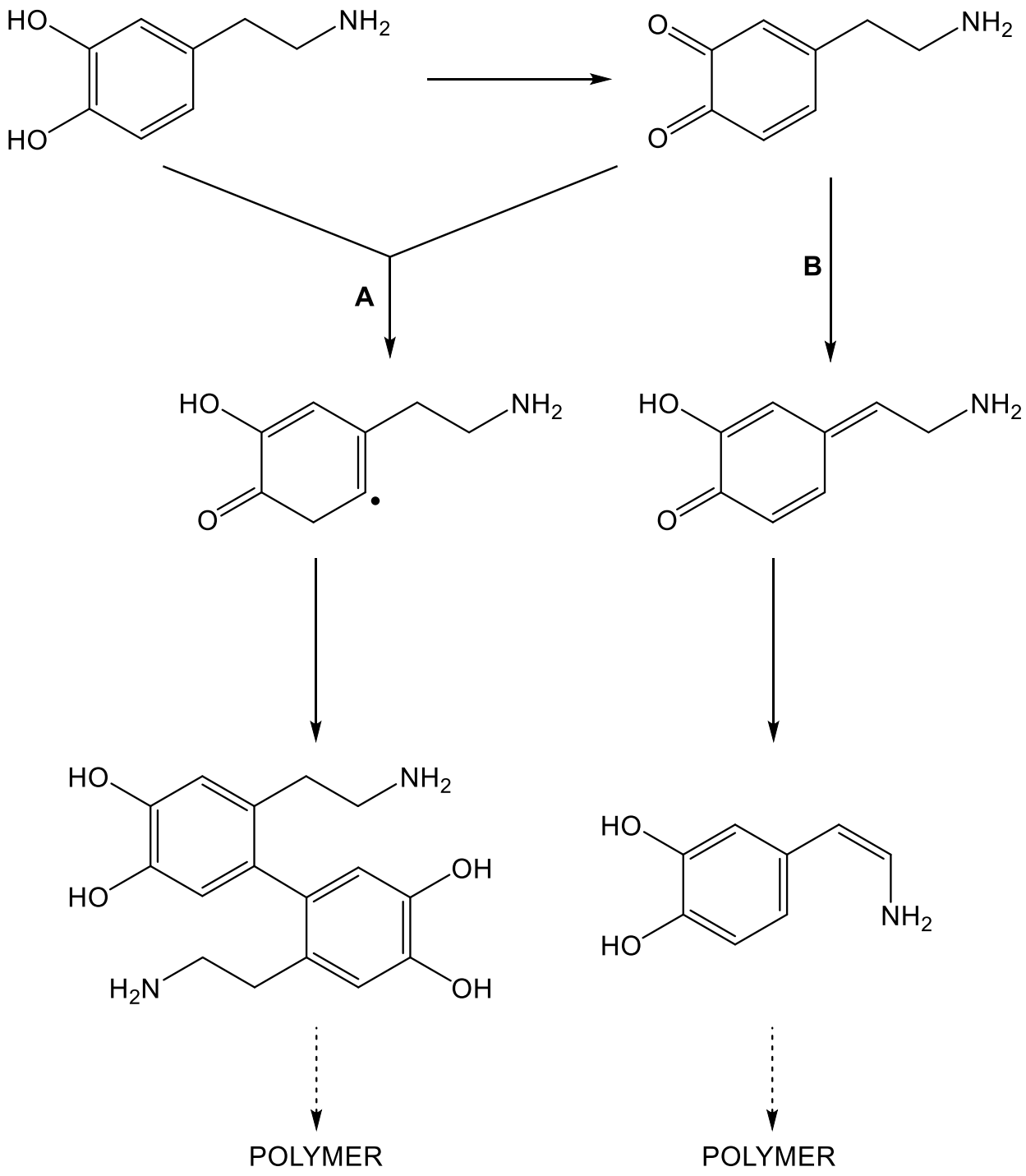

Scheme 1.7. Crosslinking pathways of *o*-quinones. **(A)** dismutation and **(B)** tautomerization. (Adapted with permission from Reference 26. Copyright 2014 Royal Society of Chemistry).

Several pathways through which PDA polymerizes have been proposed. While there is much evidence that the formation of PDA proceeds in a similar fashion as the biosynthesis of eumelanin in its initial stages, the latter stages of the polymerization mechanism remain unclear for both materials despite decades of study. Nevertheless, dissent regarding the structure and mechanism of PDA provides a frontier for further investigation.

1.1.3 Role of Metal Ions in PDA Formation

It has been postulated that metal ions, namely Fe(III), play a key role during the crosslinking of catecholic compounds in natural systems.[26] Molecules with catechol functionalization can chelate Fe(III) reversibly and non-covalently *via* one of three binding modes, forming either mono-chelated, bis-chelated, or tris-chelated complexes (Scheme 1.8).[36] The catechol to iron binding ratio is ostensibly dependent on pH through the deprotonation of catecholic hydroxy groups. In a 3 : 1 catechol : Fe molar ratio using $FeCl_3$ dissolved in a catechol-functionalized polyethylene glycol solution, predominantly mono-chelated complexes were present at pH < 5.6, bis-chelated complexes were prevalent at 5.6 < pH < 9.1, and tris-chelated complexes were principally present at pH > 9.1. It should be noted that the solubility of Fe(III) is very poor, particularly at higher pH, and must therefore be pre-bound to the catechol ligands before increasing pH.[37] It was proposed that the binding mode may also depend on the concentration of iron. In reaction systems with lower iron concentrations, the tris-chelated complexes were more prevalent, whilst at higher concentrations of iron, the mono-chelated complexes prevailed.[38]

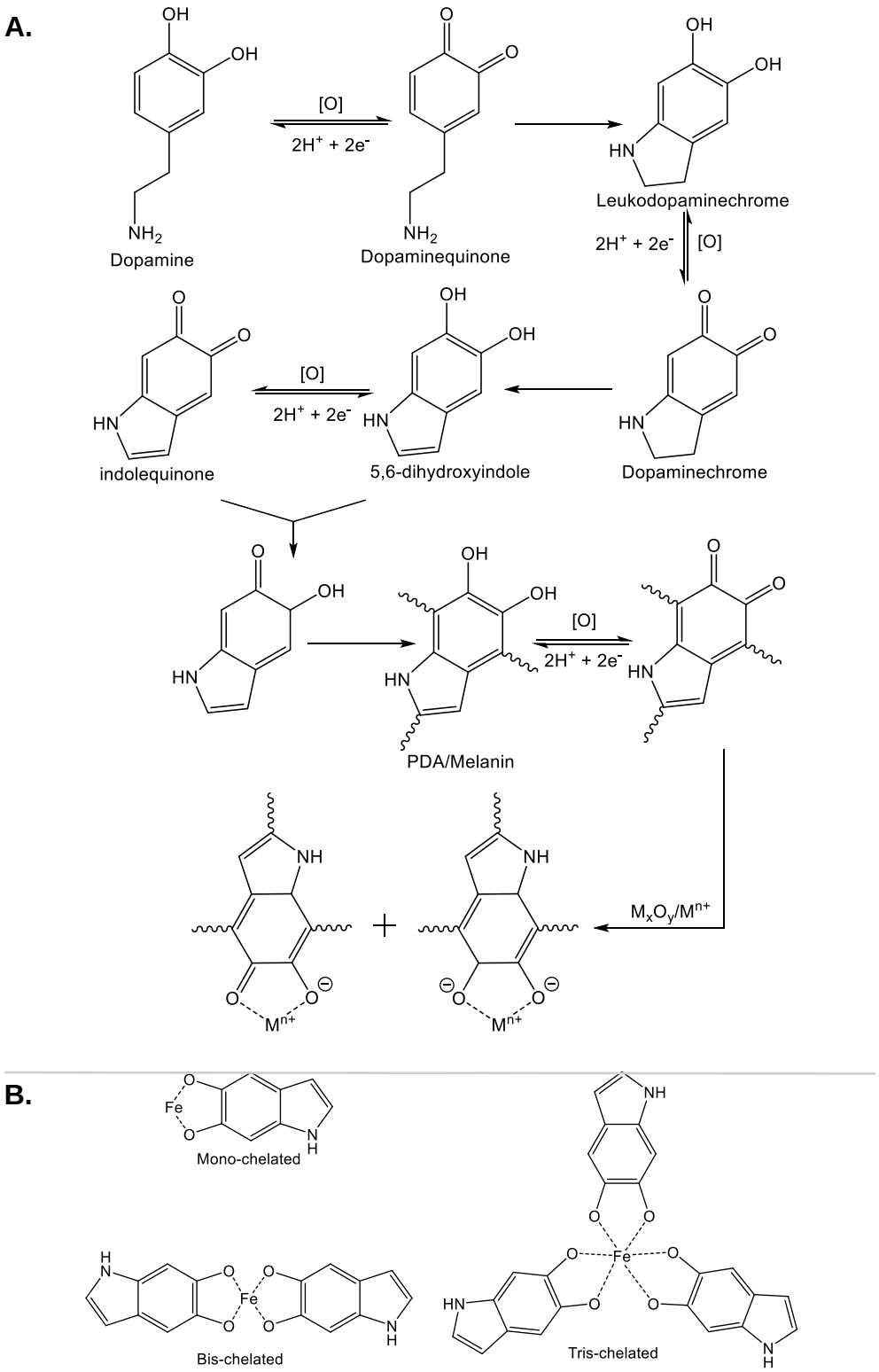

Scheme 1.8. (A) Proposed mechanism of dopamine polymerization and metal chelation at the catechol sites. (Adapted with permission from Reference 39. Copyright 2010 Elsevier) **(B)** Mono-, bis-, and tris-chelated Fe-catechol complexes.

In a study by Sun *et al*. published in 2018, a metal organic framework (MOF) of iron(III)-1,3,5-benzenetricarboxylate (Fe-BTC) was loaded with a PDA composite to serve as a water purification method. To characterize their material, attenuated total reflectance infrared (ATR-IR) and Raman spectroscopies were used to analyze the interaction of the polymer with the open iron(III) sites in the MOF. IR spectra of the PDA material revealed a peak around ~1506 cm^{-1}, suggestive of an indoline stretching vibrational mode. When the PDA composite was incorporated into the Fe-BTC MOF, this band was split into two peaks at ~1482 and ~1556 cm^{-1}, characteristic of the formation of an Fe^{3+}-PDA complex. Raman spectroscopic analyses revealed a peak around ~642 cm^{-1}, indicating the presence of Fe^{3+}-catecholate vibrational stretches, thus corroborating their IR spectroscopy findings.[40] It has also been proposed that Fe(III) may expedite catechol oxidation – the oxidation of the catechol and the reduction of Fe(III) occur at comparable potentials (~0.75V) due to their similar reduction potentials; chelated moieties may then form crosslinks upon further reaction.[41] Similarly, tris-dopa-Fe^{3+} complexes may undergo valence tautomerization, where Fe(III) is reduced to Fe(II), while dopa is oxidised to a semiquinone radical, which may then react with O_2 to produce other radical species that can couple to induce polymerization *via* crosslinking.[42,43]

A 2016 study by Li and Xie *et al*. utilised a unique approach to characterizing the elusive structural nature of PDA in which the polymer was doped with iron at varying concentrations, allowing the material to be examined *via* magnetometry. It was found that the product of magnetic susceptibility and temperature per mole iron ($\chi_M T$) of lowest iron-loaded sample at 300 K approaches that of a spin-only, purely Fe(III)-containing sample (4.375 emu K cm^{-3} mol^{-1}), eliminating the possibility of Fe(II) and low-spin Fe(III) populations, as these valences would bring about substantially different $\chi_M T$ values. The $\chi_M T$ of the highest iron-loaded sample at 300

K, however, shows greater deviation from the spin-only expectation, likely due to the higher percent coupling of the metal ions. The magnetic results of this study will be further discussed in Chapter 3. Provided the pH of the system and high concentration of dopamine used in this study, it would be assumed that a tris-catechol binding mode should be favorable in the final product. Unexpectedly, magnetic analysis, corroborated by UV-Vis spectroscopy, strongly suggested that the Fe(III) ions were predominantly coordinated in the mono-chelated binding mode.[44]

While catechol-functionalized molecules can interact with a number of other metal ions, preparation of PDA with high and tunable metal loadings beyond iron has proven challenging. In a study by Wang and Xie *et al*., a variety of metals – including Mn(III), Fe(III), Co(II), Ni (II), Cu(II), Zn(II), Ga(III), Ti(IV), V(III), Cr(III), and Gd(III) – were tested to determine the versatility of their prepolymerization loading strategy (discussed in further detail in Chapter 2). Of these, all but Ti(IV), V(III), Cr(III), and Gd(III) were found to be compatible. Consequently, metal chelation in any capacity *via* the catechol functionalization of PDA is of particular interest because of a similar metal sequestration capability in natural melanins, which may provide insight for the complex structural nature of these polymers, as well as the myriad of functionalities, and subsequently applications, of natural systems.[45]

1.2 Applications of Synthetic Melanin Materials

Although the structure of natural and synthetic melanins and the pathways through which they form are still being studied, the properties and applications of these materials have been studied extensively. Interest in the material was first inspired by the extraordinary ability of mussels, barnacles, sea urchins, star fish, and other marine organisms to securely affix themselves to rock formations. Designing materials to mimic this ability, which arises from adhesive proteins containing DOPA residues remains an active area of research.[43] Further study of structure and

function has led to biomedical applications, such as drug delivery and biosensing, due to its remarkable biocompatibility and dispersibility in water, allowing hydrophobic pharmaceuticals to be solubilized. Furthermore, synthetic melanins have been used for applications in energy, such as batteries and catalysis, due to their electrical conductivity as an organic semiconductor, as well as applications in water treatment, as a result of their ability to sequester metals and organic pollutants owing to their catechol functionalization.[10]

1.2.1 Adhesive Properties and Applications

Synthetic melanins are versatile materials that share a variety of properties with natural melanins, most notably, their adhesive properties. More specifically, there are two types of bioadhesion: temporary adhesion, witnessed in geckos scaling up surfaces, and permanent adhesion, seen in marine organisms.[46] For example, the Common Blue Marine Mussel uses the adhesive protein Mefp-1, containing numerous catechol functionalities due to the presence of DOPA. It was previously speculated that both DOPA and lysine residues were responsible for the protein's adhesive capabilities; however, it was found that DOPA was principally involved. Furthermore, DOPA is thought to contribute to the crosslinking of the organism's byssal threads and consequently, its adhesion to the bedrock. The remarkable adhesive properties in mussels and other marine organisms have served as the inspiration to a number of studies by material scientists, particularly due to the challenge of achieving water-resistant, biodegradable coatings and adhesives. Apart from the substratum to which these organisms affix themselves, the DOPA residues in the Mefp-1 protein was also found in a 1999 study to adhere to gold substrates, after which it was speculated that, because the catechol moiety has a particular affinity for Fe(III), Ag, and other metals, the protein, and consequently its synthetic analogues, would adhere to such metals.[47] In general, mussel adhesive proteins (MAP) are secreted from the organism as a fluid

that undergoes a hardening reaction *in situ*. The DOPA residues in the proteins are believed to be involved in intermolecular crosslinking reactions that result in the formation of a solid adhesive plaque. The mechanism of this crosslinking reaction is not yet unambiguously understood, but evidence suggests that crosslinking can occur either with other DOPA residues *via* radical mechanism or through Michael addition reactions with an amine functional group. Efforts to mimic the adhesive characteristics of this natural system have resulted in the incorporation of DOPA into the backbones, sidechains, and end groups of synthetic polymers. One such example is the polyethylene glycol (PEG)-DOPA macromer, which was synthesized and examined for its capability of forming hydrogels upon the addition of oxidants. The adhesive properties of this material, found to form rapid and tunable hydrogels, were proposed to be further applied for biomedical purposes.[48]

Another such example is the DOPA-modified triblock copolymer, which were synthesized to form adhesive hydrogels, proving to be a promising candidate for further application as adhesive biomaterials for tissue repair and regeneration. For this material, DOPA-containing peptides were coupled to a central PEG segment of the triblock copolymers. This new synthetic strategy provides a tunable method which facilitates control over the peptide composition, as well as the DOPA concentration. This material was designed to rapidly form hydrogels *via* photopolymerization of the methacrylate end groups upon exposure to long-range wavelength UV radiation, biodegrade through the hydrolysis of polylactic acid (PLA) segments, and enhance the adhesive properties of the resulting hydrogel material. One limitation of this strategy is the incorporation of DOPA into a gel *via* free radical polymerization, which has proven problematic due to the catechol side-chain's ability of radical quenching. Nevertheless, aqueous solutions of the peptide-modified block copolymer were found to undergo rapid photopolymerization into hydrogels through its DOPA

residues. Moreover, the wet adhesion of these hydrogels onto metal oxide surfaces can be significantly enhanced when functionalized with DOPA-containing peptides.[49] The oxidation of DOPA plays an interesting role in adhesion with respect to the substrate. In relation to inorganic surfaces, the oxidation of the catechol moiety reduces the functional group's adhesive properties, but enhances them with respect to organic substrates, likely due to the material's capacity to adhere to the surface *via* covalent bonding. This greater understanding of catecholic molecules has allowed further investigation for promising medical applications in anchoring synthetic and biological macromolecules onto metal oxide surfaces.[46]

The adhesive properties of synthetic melanins additionally show promise in applications for surface modification. Due to their versatile functionality, catechol moieties can adhere to low surface energy substrates, like Teflon or the waxy surface of a cherry tomato (Figure 1.1), allowing these surfaces to become substantially more hydrophilic. The catechol groups can also serve as a modification site for block copolymer lithography once adhered to the material.[50]

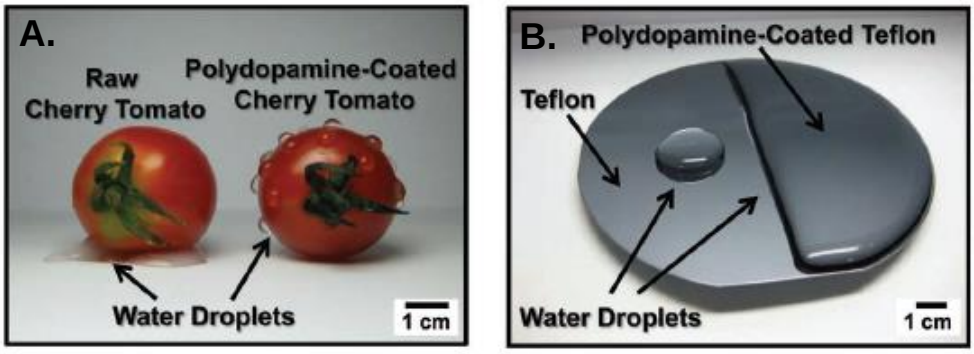

Figure 1.1. Digital images of **(A)** an coated plain cherry tomato on which droplets of water have not adhered (left) and a PDA-coated cherry tomato onto which beads of water have adhered to the surface (right); **(B)** an uncoated Teflon substrate in which droplets of water amass together on the hydrophobic surface (left) and a PDA-coated Teflon substrate on which droplets of water spread throughout the entire coated surface. (Reprinted with permission from Reference 50. Copyright 2011 John Wiley & Sons, Inc.).

Material scientists have gleaned much inspiration from the byssal threads of marine organisms to emulate their extraordinary adhesive properties, which show great promise in further

applications, like surface modification and biomedicine. Undeniably, these investigations have led to other remarkable discoveries of the countless applications of this versatile material.

1.2.2 Biomedical Applications

Investigation of PDA's adhesive properties have pioneered the studies for several other functions of the material, namely its applications in the biomedical sciences. Two notable examples are its utilization in drug delivery and biosensing.

Drug Delivery

Synthetic melanins, due to their biocompatibility and versatile functionality, are strong candidates as vessels for drug delivery, whether as a surface modifier or as the vessel itself. For instance, graphene oxide can be reduced by dopamine, after which DA is polymerized and adhered to the surface of the reduced graphene oxide (RGO). Pharmaceuticals, such as heparin (an anti-clotting drug), can then be grafted onto the PDA-functionalized surface of the material. This method is facile, safe, and green, proving to be a promising contender of drug delivery.[51]

Another exemplary use of PDA as a drug delivery method is in iron-doped PDA nanoparticles grafted with natural glucose oxidase (GOD), which results in a cascade catalytic nanomedicine specifically targeting the glucose found in tumor microenvironments (TME). The GOD grafted on the Fe-PDA nanoparticles is intended to catalyze the copious glucose in TME to gluconic acid and hydrogen peroxide. The hydrogen peroxide, in turn, is capable of enhancing the efficiency of the Fenton reaction, consequently producing hydroxyl radicals, which can then be used for cancer therapies.[52]

Biosensing

Magnetic Resonance Imaging (MRI) Contrast Agents

Synthetic melanin-based materials are of particular interest as MRI contrast agents, attributed to their biocompatibility, as well as their ability to chelate paramagnetic metal ions necessary for MR imaging. The catechol functionality of the material serves as a scaffold for metal ion coordination. In a 2016 study by Li and Xie *et al.*, PDA nanospheres were doped with Fe(III) ions. It was concluded that since high Fe(III) loading results in reduced moment per iron center, decreasing the antiferromagnetic coupling between the metal centers would ostensibly increase the sample's magnetic moment, thereby improving the signal. The proposition was made to disrupt the antiferromagnetic coupling by creating an alternate, small spin magnetic coupling channel between an Fe(III) center and an organic radical electron, or with a $S = 1/2$ transition metal, such as Cu(II).[44] In the following year, Wang and Xie *et al*. extended the study to other transition metals, such as cobalt and manganese. Their magnetic studies confirmed that controlling and diminishing the antiferromagnetic coupling between metal centers improves the material's performance as an MRI contrast agent.[45]

In the same year, Wang, Carniato, and Xie *et al*. published a study incorporating gadolinium ions into the PDA scaffold for high relaxivity MRI contrast agents. Gadolinium was a promising contender to increase the signal intensity due to its increased paramagnetic properties ascribed to its half-filled f-orbitals. Additionally, the antiferromagnetic coupling was found to be reduced in these materials due to the poorly efficient superexchange through these f-orbitals. However, at the time of publication, Gd-based contrast agents were not nearly as efficient as predicted by theoretical models, primarily due to low hydration states and rapid molecular tumbling, resulting in reduced sensitivity of detection. Gd-doped PDA nanoparticles as a new

approach offered a number of advantages: i) crosslinking of Gd-catechol chelates leads to slow molecular tumbling, increasing the contrast for MR imaging; ii) free rotation of the chelates is limited, which in turn extends to surface-bound Gd ions due to its crosslinked nature within the PDA scaffold; iii) the catechol moieties in the crosslinked network are strained, and as consequence, the formation of unsaturated Gd-catecholate complexes allows for high hydration states. This application can potentially be utilized for tumor imaging due to the improved permeability and retention effect of the material.[53]

Ultrasound (US) Contrast Agents

Ultrasound contrast agents operate by generating contrast against surrounding tissue by non-linear resonance interactions with impinging ultrasound waves. Unlike MRI contrast agents, to achieve strong signal to noise ratios, US contrast agents do not require magnetic properties, nor do they require radioactive properties like positron emission tomography-computed tomography (PET/CT). Currently, US agents that are clinically used are inert perfluorocarbons (PFC) with relatively low boiling temperatures, stabilized within a protein or phospholipid coating. A new approach to US contrast agents published by Xie *et al*. in 2018 involves the functionalization of surface of PDA nanospheres with perfluorocarbons. The size tunability and surface functionalization, as well as the metal chelation capabilities, of this material provide a broad variety of potential applications in multimodal imaging, targeted delivery, and therapeutic functionality.[54] The Doppler imaging lifetime of this material was later improved six-fold as compared to that of its predecessor by doping the material with Fe(III) ions, generating an enhanced photoacoustic (PA) signal in addition to its US signal.[55]

The uses of polydopamine in biomedicine are incredibly multifunctional, from surface modification of drug delivery systems and acting as a drug delivery system to MR and US imaging,

among several others. Utilization of this material appears to be particularly advantageous, due to its biocompatibility and versatile functionalities. Nevertheless, a deeper understanding of the polydopamine's form may allow for greater tunability of the material's function.

1.2.3 Applications in Energy

Batteries

The use of lithium-ion batteries (LIB) has become prevalent in portable electronic appliances due to their high energy densities and prolific cycle lives. However, in order for their use to be extended to larger applications, such as sustainable transportation in electric vehicles, their performance in energy density, power density, cycle lives and safety must be substantially improved as the gravimetric capacities of the anodes far exceed those of the cathodes.[56,57] Improving the energy density of LIB would therein require new electrode materials with higher specific and volumetric capacity. Alloy-type anodes, such as silicon-based anodes, have much higher Li storage capacity as compared to the intercalation-type graphite anodes that are currently used. Nevertheless, these silicon-based electrodes must have a high capacity, long cycle life, high efficiency, and industrially scalable fabrication in order to be used for practical applications. To that effect, commercially available Si nanoparticles were encased inside a thin, conformal, self-supporting carbons shells of PDA, designed with a void space between the particles and the shell, allowing for expansion of the Si nanoparticles without distorting the structure of the PDA shell or disrupting the SEI on the outer surface. This "yolk-shell" electrode design has been found to be scalable, electrochemically stable, and highly efficient.[58]

While much of the research devoted to improving the properties of LIB have focused on electrode materials, a different methodology proposes the use of PDA-coated polyethylene (PE) separators. PE separators are the most commonly used variety for commercial LIB due to their low

cost, appropriate mechanical strength and pore structure, electrochemical stability, and thermal shutdown properties. However, the use of PE is not without its limitations: the material has intrinsically poor compatibility with conventional liquid electrolytes, attributed to its hydrophobic surface character and low surface energy, resulting in poor wetting ability. Nevertheless, the surface of PE can be modified with PDA, offering electrolyte wetting capabilities, uptake of electrolytes, and ionic conductivity. Furthermore, PDA treatment is fully compatible with a broad variety of PE separators without compromising the advantageous properties of the original material.[56] To further improve the power and safety of these materials, the PE separators can be coated with dimethylaminoethanethiol (DMAET), functionalized with PDA, and treated with a final coating of silica. In this case, PDA in pivotal in that it mediates robust adhesion of the hydrophilic ceramic layer, which lacks polymeric binders (thereby having adverse effects on ion transport), to the hydrophobic PE surface. The material overall exhibits an improved rate performance and thermal stability as compared to the uncoated material.[59]

The consequential uptake of electrolytes due to the hydrophilicity of PDA, in turn, enables a well-distributed Li-ionic flux which encompasses the entirety of the Li-metal surface, thereby reducing Li-dendrite growth. The growth of dendrites can result in exhaustion of the electrolyte or limited diffusion of Li owing to over-thickening of solid-electrolyte-interphase (SEI) layers. Moreover, the PDA coating of separators improves the intrinsic thermal-shrinkage issue of these materials and addresses an imperative safety issue, as thermal shrinkage may result in short circuiting between the cathodes and anodes, eventually causing the cell to explode.[57]

Supercapacitors

Comparatively, supercapacitors maintain a number of properties which are not currently attainable for batteries, such as higher power densities, sub-second charging, sustained cycle life,

and an immensely broad range of temperature at which they can operate. Polydopamine's role in these supercapacitors is to serve as a carbon source for enhancing the conductivity of these materials.[10] One such example of a PDA-treated supercapacitor is a one-dimensional, highly graphitic, carbon-tipped manganese oxide/mesoporous carbon/ manganese oxide hybrid nanowire, whose structural design was intended to improve the conductivity of metal oxide materials. Manganese oxides are considered to be a promising contender for next-generation transition metal supercapacitors due to their low cost and environmental benignity. For these supercapacitors, PDA is used as a coating on the nanowire, allowing the material to withstand temperatures up to 800ºC in an inert atmosphere. Additionally, the catechol moieties can coordinate with Mn^{2+} to form Mn-based complexes within the material. As a whole, these nanowires have shown to be high-performance supercapacitors that address the potential issue of poor conductivity.[60]

1.2.4 Applications in Water Treatment

Metal Sequestration

The contamination of drinking water with heavy metals, especially lead, is an incessant global problem resulting in severe public health consequences. Materials which incorporate PDA, capable of scavenging metals due to its amine and catechol functionalities within its matrix, have been proposed as promising potential applications to address this pervasive issue. For example, the inexpensive, water-stable MOF/polymer composite, Fe-BTC/PDA, exhibits rapid and selective removal of heavy metals, including Pb^{2+} and Hg^{2+}. The tunability, regeneration, and separation of this composite are facile, and the material is high-performing, such that within 1 minute of exposure to 1000 ppb of Hg^{2+} and Pb^{2+}, the material can reduce concentrations of these metals by approximately 99% (1.2 and 1.6 ppb, respectively).[40] Another such example is the sequestration of Cu^{2+} ions from aqueous solutions. There is a major release of copper to water supplies from the

paint, metallurgy, chemical manufacturing, and mining industries, among others, and while copper is a biologically essential metal in low doses, in higher quantities, the metal becomes toxic. PDA nanoparticles are promising contenders for the treatment of wastewater, as they are biodegradable and nontoxic, as well as effectively remove Cu^{2+} ions from aqueous solutions.[61]

Organic Pollutant Sequestration

In addition to heavy metal contamination, organic pollutants, such as Rhodamine B, can be found in wastewater. Carbon-based nanomaterials, particularly carbon aerogels, carbon nanotubes (CNT), graphene, and other composites have demonstrated their abilities in the removal of organic pollutants, though their lack of surface functional groups poses a stark limitation. This shortcoming can be remedied by introducing organic functionalization or metal oxide nanoparticles; however, recovery of these materials may cause concern due to possible unforeseen environmental side effects if not completely removed. To address this issue, a free-standing graphene hydrogel was modified with PDA for use in water purification. In the fabrication of this material, DA acts as both a reductant and a functionalization agent for graphene oxide (GO), whilst graphene nanosheets are assembled into 3-dimensional structures. In this case, PDA is expected to provide the active sites for synthetic dyes and other organic pollutants through hydrogen bonding interactions. It was found that this composite can be easily regenerated using low-cost reagents and is effective in the uptake of Rhodamine B, exhibiting a high adsorption capacity after several absorption/desorption cycles.[62]

Another example is a clay-based hydrogel modified with PDA and Fe^{3+} ions in which PDA self-assembles within the clay hydrogel (D-clay) and acts as the main building block, and the iron ions serve as physical crosslinkers. The coordination interactions between the D-clay nanosheets and the iron ions results in a supramolecular network that can effectively remove Rhodamine 6G

(Rh6G) from water due to complexes formed between D-clay and Rh6G *via* hydrogen-bonding and π-π stacking interactions. This alternative is also low-cost, scalable, and environmentally benign.[63]

Desalination

Water purification and desalination of drinking water by reverse osmosis and nanofiltration have demonstrated their remarkable capability of effectively removing low molecular weight impurities from water sources. However, these processes are incredibly energy-intensive, and improvements to make them more sustainable are urgently needed. Inspired by aquaporins, water channel proteins in biological membranes with extraordinary water permeability and selectivity, PDA-coated AquaporinZ (AqpZ) is a potential application in pressure-driven water purification. PDA is known to react with amine- and thiol-containing compounds, thereby facilitating the grafting of additional layers onto its surface. The nanofiltration membrane was fabricated but immobilizing vesicles onto a porous membrane through the formation of adducts and can withstand immense hydraulic pressures. Additionally, the material exhibits higher pure water permeability and rejection of NaCl and $MgCl_2$ salts.[64] Similarly to other material composites, PDA can be used to modify the surface of polysulfone (PSf) substrates, over which *m*-phenylenediamine (MPD) and trimesoyl chloride (TMC) are employed as monomers for interfacial polymerization to form a polyamide rejection layer. Not unlike other aforementioned materials in previous sections, PDA-modification produces a smooth hydrophilic surface comprised of smaller surface pores with a narrow pore size distribution, which may prove to be favorable for the fabrication of a better quality polyamide layer, and as consequence, enhanced salt rejection.[65]

1.2.5 Objective

It is evident that PDA is an extensively studied material and demonstrates extraordinary versatility in its application. To optimize tunability of the properties of PDA, it is critical to understand the crosslinking mechanism of this material. The structure of PDA has yet to be unambiguously understood, despite the countless studies, which have been conducted to structurally characterize this amorphous polymer. Of these, magnetometry is a unique method which may potentially uncover further insight on the local structure, as well as other emergent properties of this material. The primary study in this manual investigates the electronic structure implications resulting from small variations in the synthesis of synthetic melanin materials. The results of this work are described herein.

CHAPTER 2: MATERIALS AND METHODS

2.1 Synthetic Strategies: General Procedures

Chemicals were purchased commercially and used without further purification. Deionized water was used for all syntheses. The reaction schema for each synthetic strategy is illustrated in Scheme 2.1.

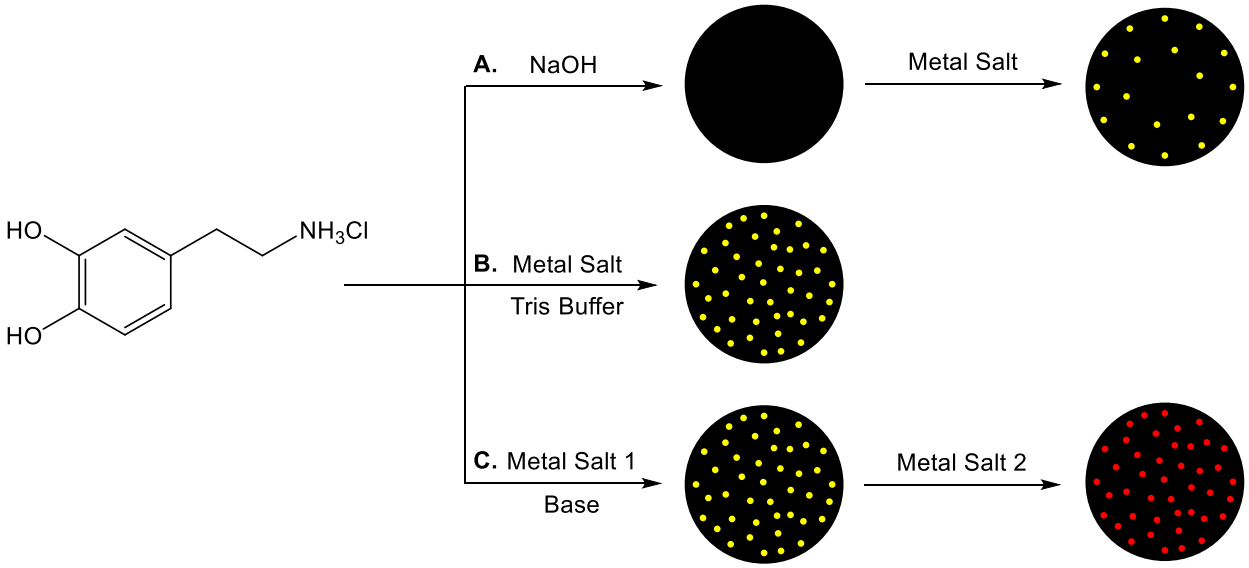

Scheme 2.1. Reaction schema for **(A)** post-polymerization metal-doping strategies, **(B)** pre-polymerization metal-doping strategies, and **(C)** metal ion exchange strategies (Adapted with permission from References 45 and 46. Copyright 2017 American Chemical Society, Copyright 2017 John Wiley & Sons, Inc.).

2.1.1 Preparation of PDA Nanospheres

Polydopamine nanospheres can be used as a template in which metal ions can be loaded post-synthesis. This material was prepared using a modification of a previously published method (Scheme 2.1A).[66]

Dopamine hydrochloride (DA•HCl, 200 mg) was dissolved in deionized water (100 mL) with vigorous stirring for 30 minutes. Aqueous 1M sodium hydroxide (NaOH, 1.06 mL) was then charged into the reaction flask, resulting in a color change from clear colorless, to yellow, to red-orange, to brown, to a cloudy, black nanoparticle suspension, which was left to stir vigorously for 24 hours in ambient atmosphere. The nanoparticles were isolated *via* centrifugation, washed with three portions of deionized water (3 × 20 mL), and stored as a concentrated nanoparticle suspension.

2.1.2 Preparation of Mn(III)-doped PDA Nanospheres

Mn(III)-doped PDA nanospheres were synthesized as a precursor for the preparation of Fe(II)-doped PDA nanoparticles and were prepared using a previously published pre-polymerization strategy (Scheme 2.1B).[45]

DA•HCl (300 mg) and manganese(III) acetate tetrahydrate ($Mn(OAc)_3•4H_2O$, 150 mg) were dissolved in deionized water (1000 mL) with vigorous stirring for 30 min. A basic buffer solution was prepared by dissolving Tris powder (10 g) in deionized water (500 mL) with gentle swirling. The buffer solution was then poured into the reaction flask, resulting in a color change from clear colorless, to yellow, to orange, to brown, to a cloudy black nanoparticle suspension, which was left to stir vigorously for 24 h under an ambient atmosphere. The nanoparticles were isolated *via* centrifugation, washed with three portions of deionized water (3 × 20 mL), and stored as a concentrated nanoparticle suspension.

2.1.3 Preparation of Fe(II)-doped PDA Nanospheres

Fe(II)-doped PDA nanospheres were prepared under an inert atmosphere of argon using standard cannula and Schlenk techniques, following the previously published cation exchange procedure with modifications (Scheme 2.1C).[46]

An iron(II) salt solution was prepared with anhydrous $FeCl_2$ (500 mg, used as is) and deoxygenated water (25 mL). To an aliquot of the Mn-doped PDA nanoparticle suspension was added 10 mL of the iron salt solution, which was left to react for 24 h with vigorous stirring. The product was isolated *via* centrifugation, washed with 3 portions of water (20 mL) and reacted with a second portion of the iron salt solution (10 mL) for an additional 24 h with vigorous stirring. The nanoparticles were isolated *via* centrifugation once more, washed with three portions of deionized

water (20 mL), and stored as a concentrated nanoparticle suspension to be further analyzed in future studies.

2.1.4 Preparation of Fe(III)-doped PDA Nanospheres

Fe(III)-doped PDA nanospheres were prepared using a modification of a previously published method.[44] DA•HCl (30 mg) and $FeCl_3$ (10 mL, anhydrous) were dissolved in deionized water (100 mL) for 30 min with vigorous stirring, producing a dark blue-green solution. A basic buffer was prepared by dissolving Tris powder (1 g) in deionized water (50 mL) with gentle swirling. The buffer solution was then poured into the reaction flask, changing color to dark burgundy and then to the cloudy black nanoparticle suspension, which was left to react for 24 h with vigorous stirring. The nanoparticles were isolated *via* centrifugation, washed with three portions of deionized water (20 mL), and stored as a concentrated nanoparticle suspension to be further analyzed in future studies.

2.1.5 Preparation of Fluorinated PDA Nanospheres

PDA nanospheres were prepared as a precursor using the synthetic methods described in Section 2.1.1. Fluorinated PDA nanospheres were prepared using a modification of a previously published method.[54] An aliquot of the polydopamine nanoparticle suspension (40 mL) was mixed with 10 mL of ethanol with vigorous stirring for 10 min. A 60 μL portion of 1H,1H,2H,2H-perfluorodecanethiol was charged to the reaction flask and continued to stir for an additional 5 min. A basic solution was prepared by vortexing a mixture of deionized water (10 mL) and ammonium hydroxide (150 μL), which was added to the reaction mixture and allowed to react for 24 h with vigorous stirring. The nanoparticles were isolated *via* centrifugation, washed with three portions of deionized water (20 mL), and stored as a concentrated nanoparticle suspension. These materials will be analyzed further in future studies.

2.1.6 Preparation of Fe(III)-doped PDA Aggregate Materials

The Fe(III)-doped PDA aggregate material was prepared using a modification of the synthetic method described in Section 2.1.4. The variable parameters for the preparation of this material is described in Table 2.1.

DA•HCl and $FeCl_3$ (anhydrous) were dissolved in deionized water (100 mL) for 30 min with vigorous stirring, producing a dark blue-green solution. A basic buffer was prepared by dissolving Tris powder in deionized water (50 mL) with gentle swirling. The buffer solution was then poured into the reaction flask, changing color to dark burgundy and then to the cloudy black nanoparticle suspension, which was left to react for 2 h with vigorous stirring. The nanoparticles were isolated *via* centrifugation, washed with three portions of deionized water (20 mL), and stored as a concentrated nanoparticle suspension. Samples 6, 15, 17 and 26 were used for magnetic characterization (Table 2.1).

Table 2.1. Parameter variations for the preparation of Fe(III)-doped PDA aggregate materials. Samples 1-4 were prepared with varying amounts of $FeCl_3$ whilst both dopamine hydrochloride and Tris buffer amounts were held constant. Samples 5-15 were prepared by varying amounts of Tris buffer at constant dopamine hydrochloride concentrations and high concentrations of iron. Samples 16-26 were prepared by varying amounts of Tris buffer at constant dopamine concentrations and low concentrations of iron.

Sample	Mass DA•HCl (mg)	Mass $FeCl_3$ (mg)	Mass Tris (g)
1	300	100	1
2	300	50	1
3	300	25	1
4	300	10	1
5	300	100	0.25
6	300	100	0.5
7	300	100	2
8	300	100	3
9	300	100	4
10	300	100	5
11	300	100	6
12	300	100	7
13	300	100	8
14	300	100	9
15	300	100	10
16	300	10	0.25
17	300	10	0.5
18	300	10	2
19	300	10	3
20	300	10	4
21	300	10	5
22	300	10	6
23	300	10	7
24	300	10	8
25	300	10	9
26	300	10	10

2.2 Analytical Methods

2.2.1 Characterization of Material Morphology

Transmission Electron Microscopy (TEM)

Samples were prepared by drop-casting 10 μL of the diluted nanomaterial suspension onto mesh carbon film TEM grids and imaged using Fei Tecnai G2 Spirit TEM operating at 120 kV to analyze the relative density of the material.

Scanning Electron Microscopy (SEM)

Samples were prepared by drying an aliquot of the nanomaterial suspension in a vacuum oven at 70ºC. A small amount was dispensed onto carbon tape mounted on aluminum imaging stages. Images of the samples were obtained using FEI Quanta 250 SEM to analyze the surface topography of the material.

Dynamic Light Scattering (DLS)

Samples were prepared by diluting an aliquot of the PDA nanomaterial suspension. The material's hydrodynamic radii were analysed using a Malvern Zetasizer Nano ZS90.

2.2.2 Characterization of Metal Concentration

Inductively Coupled Plasma-Mass Spectrometry (ICP-MS)

Samples were prepared by digesting 1 mg of dried material in 3.5% trace metal grade nitric acid, diluted serially to various concentrations. The metal concentration of each sample was then determined by a Thermo Fisher Scientific iCAP RQ Inductively coupled plasma-mass spectrometer.

2.2.3 Characterization of Magnetic Properties

Superconducting Quantum Interference Device (SQUID) Magnetometry

Samples were prepared by loading the dried material into a polycarbonate gel capsule sealed with Teflon tape and secured in a sample straw. Magnetic analyses were conducted using a Quantum Design MPMS3 superconducting quantum interference device.

CHAPTER 3: RESULTS AND DISCUSSION

3.1 Magnetic Analysis of Fe(III)-loaded PDA Aggregate Materials

While magnetically-active metal-loaded PDA materials are complex magnetic systems, they can be modelled using a comparatively simple model which incorporates an isotropic gyromagnetic value (g = 2) and a magnetic coupling constant, J, and can be described with the Heisenberg-Dirac-Van-Vleck (HDVV) Hamiltonian (Equation 1).

$$\widehat{H} = -2J\hat{S}_1 \cdot \hat{S}_2 \qquad \text{(Equation 1)}$$

where $\hat{S}_1$ and $\hat{S}_2$ are spin operators for equivalent interacting spins.

For the case of metal-loaded PDA nanospheres, this implies superexchange coupling, in which magnetic centers couple through a diamagnetic bridge, wherein DA moieties could serve as that bridge between two metal centers.[44]

3.1.1 Isotropic Interactions Using a Dinuclear Model: Magnetic Susceptibility

To interpret the magnetic susceptibility of the metal-loaded PDA aggregated samples, it is important to determine in which oxidation state the metal centers exist. In the case of iron, the metal centers could possibly exist as Fe(II) or Fe(III), in either octahedral or tetrahedral geometries, and as either high spin or low spin complexes. Because of the tris bidentate coordination environment of the catechol ligands, tetrahedral geometries are unlikely and can therefore be eliminated as a possibility, leaving potential octahedral high and low spin Fe(II) and octahedral high and low spin Fe(III). With the model described in Section 3.1, only two types of centers are of interest: isolated centers and coupled centers. Magnetic susceptibility of a system containing only isolated iron centers can be determined by:

$$\chi = \frac{Ng^2\beta^2}{3kT}[S(S+1)] \qquad \text{(Equation 2)}$$

where χ is magnetic susceptibility, N is Avogadro's number, g is the gyromagnetic value, β is Bohr magneton, k is the Boltzmann constant, T is temperature, and S is spin. Equation 1 can be rewritten as:

$$\chi T = \frac{Ng^2\beta^2}{3k}[S(S+1)] \qquad \text{(Equation 3)}$$

which will be used for the magnetic analysis of the iron-loaded PDA samples.[67] Using Equation 2, the product of magnetic susceptibility and temperature as a function of temperature can be determined for Fe(III)O_h, h.s. (S = 5/2), Fe(II)O_h, h.s. (S = 2), and Fe(III)O_h, l.s. (S = 1/2), which turns out to be 4.375 emu K mol^{-1}, 3.000 emu K mol^{-1}, and 0.375 emu K mol^{-1}, respectively, and is illustrated in Figure 3.1.

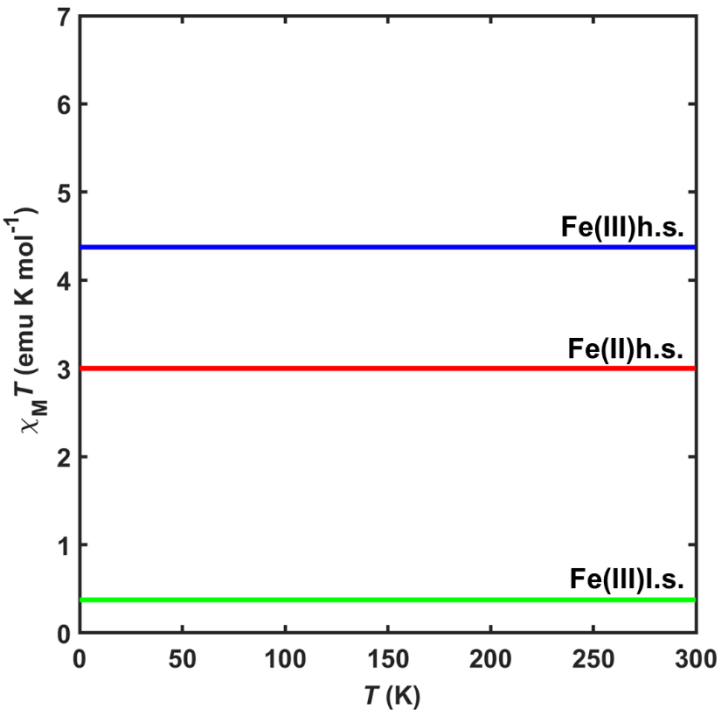

Figure 3.1. Simulation of $\chi_M T$ vs. T for isolated Fe(III), high-spin (h.s.) centers (S = 5/2), Fe(II), high spin centers (S = 2), and Fe(III), low spin (l.s.) centers (S = 1/2).

The magnetic susceptibility of a system containing only coupled centers can be determined using:

$$\chi T = \frac{Ng^2\beta^2}{3k} \frac{\sum_s S(S+1)(2S+1)e^{[-E(S)/kT]}}{\sum_s (2S+1)e^{[-E(S)/kT]}} \quad \text{(Equation 4)}$$

where $$E(S) = -\frac{J}{2} S(S+1) \quad \text{(Equation 5)}$$

When $J = 0$, there are no coupling interactions between metal centers, and therefore it can be assumed that the metal centers are isolated from each other in the system. When $J > 0$, the metal centers couple ferromagnetically to each other, where the magnetic moments of each metal center in a pair align parallel to, or in the same direction as, each other. When $J < 0$, the metal centers couple antiferromagnetically to each other, where the magnetic moments of each metal center in a pair align antiparallel, or in the opposite direction, of each other.[67] The coupling interactions of a system containing solely Fe(III)O_h, h.s. centers is illustrated in Figure 3.2.

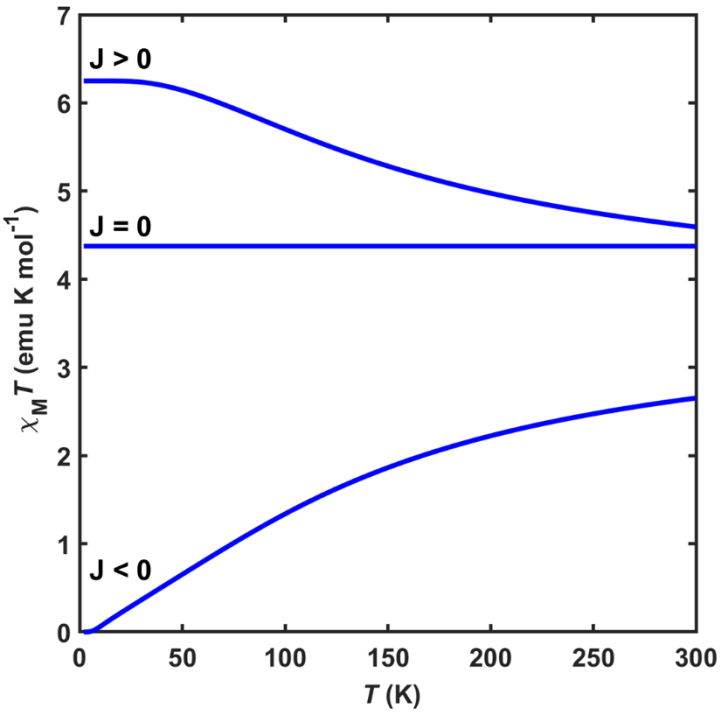

Figure 3.2. Simulation of $\chi_M T$ vs. T for an Fe(III) dinuclear compound where J is positive (ferromagnetic coupling between magnetic centers), negative (antiferromagnetic coupling between magnetic centers), and zero (isolated centers).

Systems containing only isolated centers and systems containing only perfectly coupled centers are ideal cases and are highly unlikely in case of metal-loaded synthetic melanins, especially considering the amorphous character of a largely organic polymer. While DA molecules are considered to serve as a diamagnetic bridge through which metal centers antiferromagnetically couple, it remains to be known if only one monomer of DA (or any of its analogues) bridges two metal centers or if there are circumstances in which small chain oligomers bridge two metal centers. If such is the case, it is highly likely that the coupling strength of the metal pairs would be affected as the magnetic centers are distanced farther apart within the polymer. Similarly, the percent of coupled and uncoupled metal centers can also affect the magnetic behavior of the sample. The type of coupling will determine if the magnetic susceptibility will translate closer to any of the three ideal cases. If the material is ferromagnetic, then a high percent of coupled centers will result in a higher overall magnetic susceptibility, whereas a high percentage of coupled centers in an antiferromagnetic material will result in a lower overall magnetic susceptibility. Figure 3.3 illustrates the effects of varying the coupling strength (Figures 3.3A-C) and percentage of coupled metal centers (Figures 3.3D-F) for an antiferromagnetically-coupled, octahedral, high spin Fe(III) system.

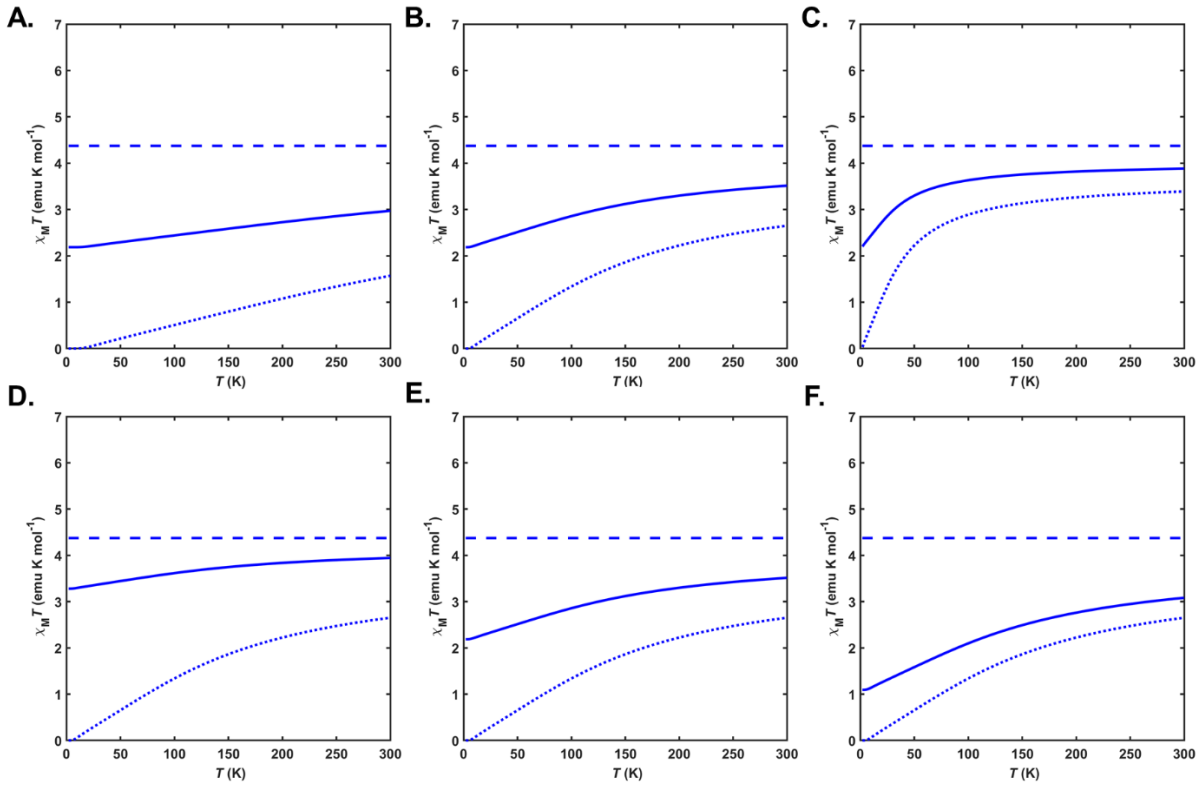

Figure 3.3. Simulated models of an Fe(III) dinuclear compound illustrating cases in which all centers are isolated (dashed) or antiferromagnetically coupled (dotted). A mix of both cases is denoted by the solid line. The gyromagnetic ratio, g = 2 for all cases. **(A)** Percent centers coupled = 50%; J = –50 cm^{-1}; **(B)** Percent centers coupled = 50%; J = –20 cm^{-1}; **(C)** Percent centers coupled = 50%; J = –5 cm^{-1}; **(D)** Percent centers coupled = 25%; J = –20 cm^{-1}; **(E)** Percent centers coupled = 50%; J = –20 cm^{-1}; **(F)** Percent centers coupled = 75%; J = –20 cm^{-1}.

It is important to note that variation in coupling strength results in a dramatic difference of magnetic behavior at low temperature with minor vertical shift in the material's $\chi_M T$, while variation in percent of centers coupled results in a vertical translation in the $\chi_M T$ of the system with little change in the magnetic behavior at low temperature.

As consequence, the model that will be applied to iron-doped PDA aggregates assumes that all metal centers within the PDA scaffold are octahedral, high spin Fe(III) which coupled antiferromagnetically to each other *via* superexchange due to the presence diamagnetic bridges between iron centers. The magnetic susceptibility of Fe(III)-PDA at varying iron concentrations and prepared with varying amounts of buffer were measured using SQUID magnetometry. The results are discussed in further detail in the following section.

3.1.2 Magnetic Susceptibility Analysis of High Iron Concentration Samples

The synthetic strategy for Fe(III)-PDA was modified such that the concentrations of the starting monomer (DA•HCl) and the iron salt were both increased tenfold (holding the buffer amount true to the original procedures), as the previously published methods posed a few limitations. While the synthesis resulted in monodisperse and uniformly-sized nanospheres, the procedures were time-consuming and low-yielding, and because only a small fraction the samples were magnetically active while the rest comprised of organic material, SQUID analysis required greater sample loading volumes. The modified synthesis produced greater yield in significantly less time. Despite the poor size distribution and poor dispersibility of the material, the results of these studies are consistent with those in the studies carried out by Li and Xie *et al*. (Figure A1), suggesting that the electronic structure of the material is independent of the interparticle interactions. It had also been concluded in their work that the coupling strength of the metal centers appears independent of the metal concentration ($J = -31$ cm^{-1}), i.e. the coupling strength for high iron loadings and low iron loadings were comparable.[44] Interestingly, the coupling strength in samples prepared with higher concentrations of Tris buffer (pH ~ 9.45) are significantly lower than those prepare with lower concentrations of Tris buffer (pH ~ 7.64), despite comparable iron loadings and percent of coupled metal centers (Figure 3.4).

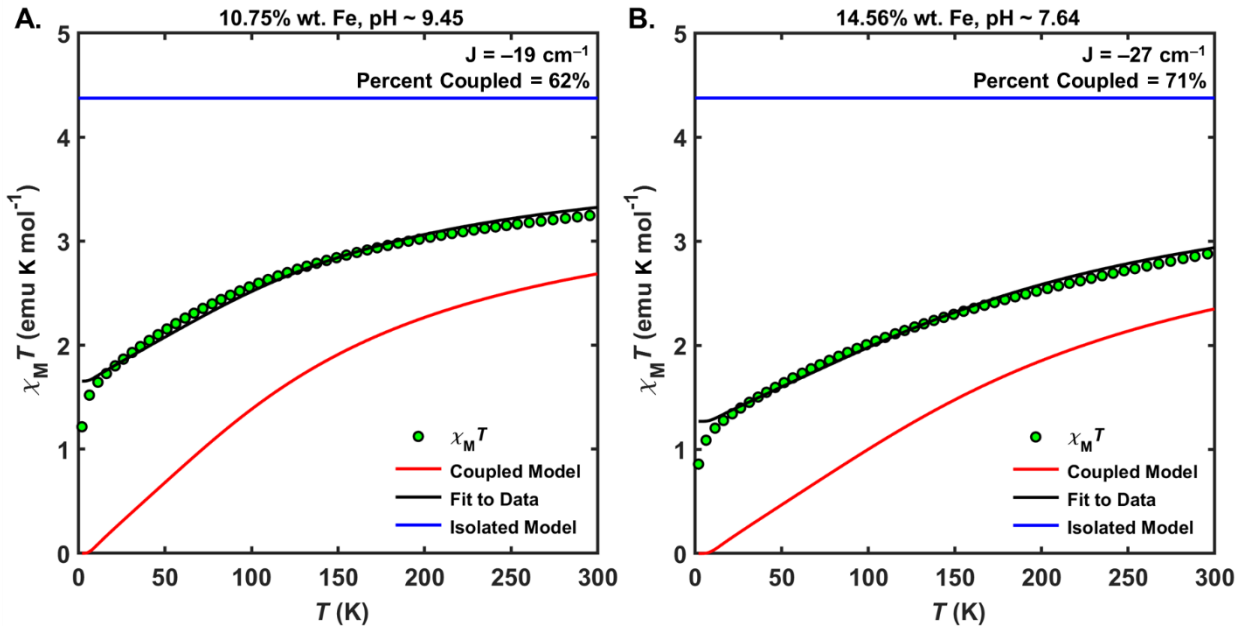

Figure 3.4. $\chi_M T$ vs. T plots of PDA with high iron-loading at **(A)** high Tris concentration (pH ~ 9.45, J = –19 cm^{-1}, Percent coupled = 62%) and **(B)** low Tris concentration (pH ~ 7.64, J = –27 cm^{-1}, Percent coupled = 71%).

The fit to the data was determined by using a non-linear least squares algorithm, Solver, to find a global minimum for the coupling strength and percentage of coupled metal centers with fixed gyromagnetic values. It is important to note that fit is, at best, an approximation, where the combination of the coupling strength and the percent coupled are one out of several possible solutions. To achieve a more accurate approximation with require further investigation.

3.1.3 Magnetic Susceptibility Analysis of Low Iron Concentration Samples

Low-iron loaded samples were prepared by increasing the DA concentration tenfold, whilst keeping the Tris buffer and iron concentrations true to the previously reported procedures. The magnetic results of these samples are also comparable to those of Li and Xie *et al*. Additionally, the morphology of these materials was consistent to those containing high concentrations of iron (Figure A2). Surprisingly, the effect of the buffer concentration on the coupling strength is dissimilar to that of the high iron loaded samples. While the antiferromagnetic coupling

interactions were strengthened with a decrease in buffer concentration in high iron loaded samples, the coupling strength is weakened at lower buffer concentrations (Figure 3.5).

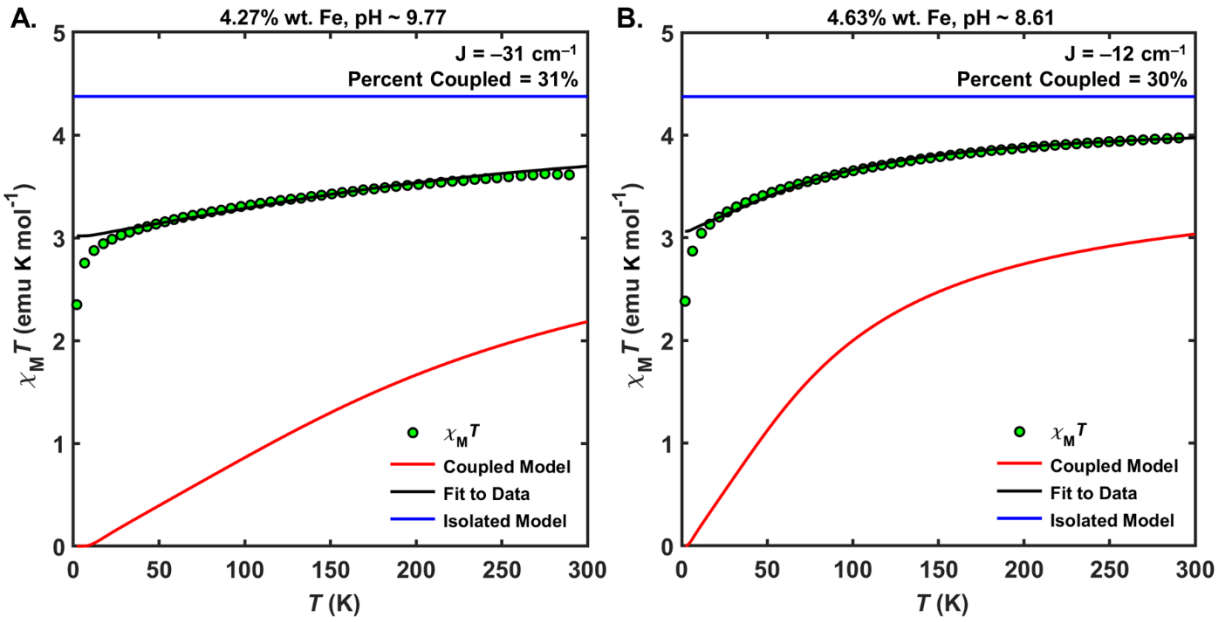

Figure 3.5. $\chi_M T$ vs. T plots of PDA with low iron-loading at **(A)** high Tris concentration (pH ~ 9.77, J = –31 cm^{-1}, Percent coupled = 31%) and **(B)** low Tris concentration (pH ~ 8.61, J = –12 cm^{-1}, Percent coupled = 30%).

The fit to the data was determined in a similar manner to the high iron loaded samples. The anomaly in the effect of the buffer concentration between samples with high and low concentrations of iron is curious and requires further investigation in order to determine a trend in the base's effect on the coupling strength, if any. Preliminary data from a study currently in progress strongly suggest that $\chi_M T$ is significantly sensitive to the concentration of iron present in the sample (data not shown). To this effect, it is imperative to optimize the quantitative methods.

3.1.4 Isotropic Interactions Using a Dinuclear Model: Magnetization

Although a simple model can be used to model the magnetic susceptibility of this complex, modelling the magnetization data for these systems is far less straightforward. All of the following simulations were generated in the program, PHI.[68] Akin to the magnetic susceptibility, it is important to consider both cases in which all metal centers in the system are isolated and in which

all centers are antiferromagnetically coupled. Figure 3.6 illustrates *M* vs. *H* simulations of these ideal cases from 0 T to 7 T.

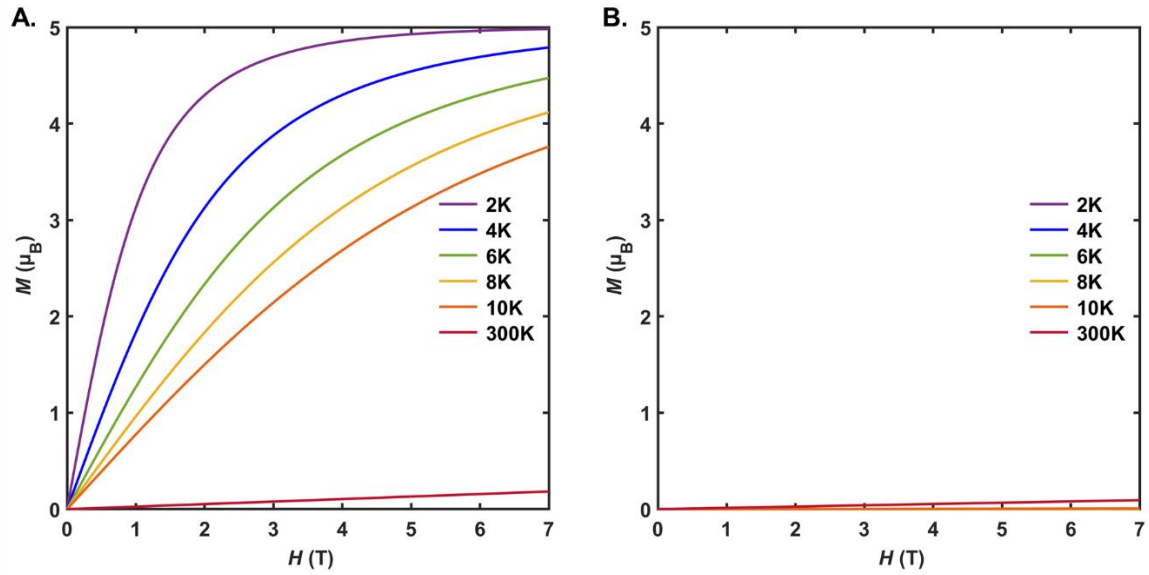

Figure 3.6. Simulated models of *M* vs. *H* plots from 0T to 7T for **(A)** a system comprised of all isolated Fe(III) (*S* = 5/2) centers and **(B)** a system comprised of all coupled Fe(III) (*S* = 5/2) centers.[68]

An important feature to note in the case of isolated metal centers is the saturation of the magnetization at low temperatures (2K). Additionally, the magnetization in the case of coupled metal centers is near zero and can barely be observed within this magnetic field range. However, the magnetic behavior in both cases becomes more apparent when the magnetic field range is broadened (Figure 3.7).

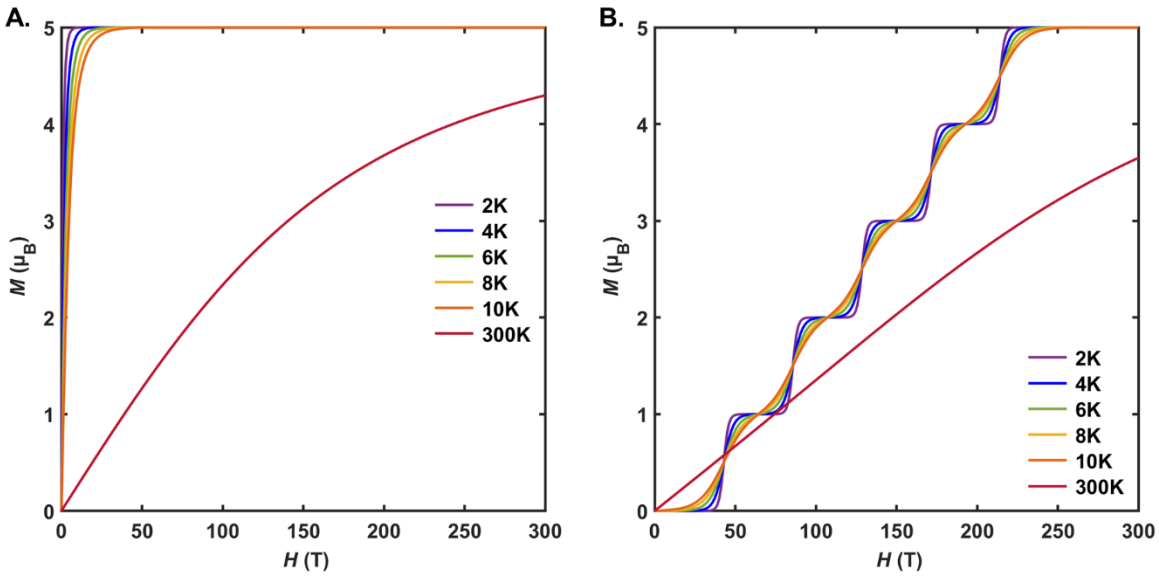

Figure 3.7. Simulated models of *M* vs. *H* plots from 0T to 300T for **(A)** a system comprised of all isolated Fe(III) (*S* = 5/2) centers and **(B)**. a system comprised of all coupled Fe(III) (*S* = 5/2) centers.[68]

The magnetic saturation in the case of isolated metal centers at all low temperatures (2K-10K) becomes more prominent at approximately 50T, while in the case of coupled metal centers, a staircase-like curve is observed. This is attributed to the change in ground state as the magnetic field is increased. However, because a magnetic field of 300T is unattainable by any instrument available for experimentation, this behavior is not explicitly observed in the data.

To achieve a model that closely resembles the data obtained, magnetization simulations can be combined in their respective coupled:uncoupled ratios. However, modelling becomes much more challenging in systems where the magnetization of the sample does not magnetically saturate at 7T. This issue can be addressed by applying an anisotropy term, *D*, which is often reported as an absolute value, as both the positive and negative value may provide a reasonable fit for powder samples in magnetometry. In the following sections, the anisotropy term is assumed to be $D = -1$ for all cases.

3.1.5 Magnetization Analysis of High Iron Concentration Samples

The simulations generated in PHI were fit to the magnetization data obtained for the high iron loaded PDA samples, using the coupling strength value and the percent of coupled metal centers approximated in the magnetic susceptibility analyses (Figure 3.8).

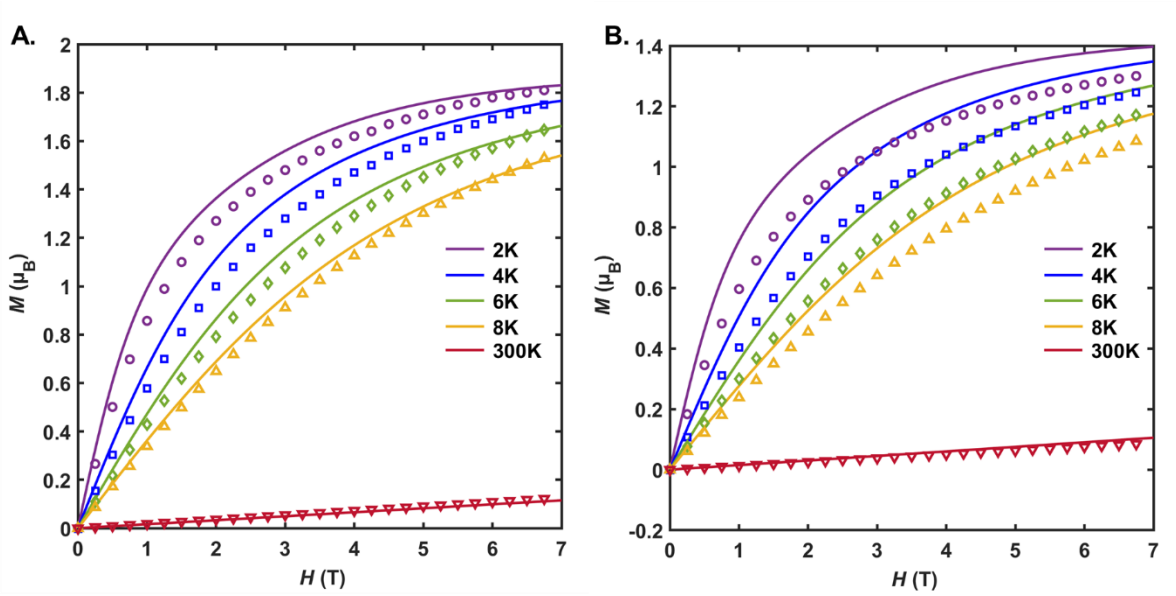

Figure 3.8. *M* vs. *H* plots fitted with PHI of high iron-loaded PDA samples at **(A)** high Tris concentration (pH ~ 9.45, $J = -19$ cm^{-1}, Percent coupled = 62%) and **(B)** low Tris concentration (pH ~ 7.64, $J = -27$ cm^{-1}, Percent coupled = 71%).[68]

A few interesting speculations can be made from these data: i). the simulation closely resembles the data in the sample prepared at high pH, suggesting that the parameters used to generate the simulation are similar to those of the actual system (i.e. coupling strength, percent coupled, anisotropy term); ii). the simulation for the sample prepared at low pH is a poor fit to the data, suggesting that the approximated parameters of the model and data are dissimilar and therefore require further optimization.

3.1.6 Magnetization Analysis of Low Iron Concentration Samples

In a similar manner as the high iron loaded samples, the magnetization data obtained for the low iron loaded PDA samples were "fit" to the simulations generated in PHI using the coupling

strength value and the percent of coupled metal centers approximated in the magnetic susceptibility analyses (Figure 3.9).

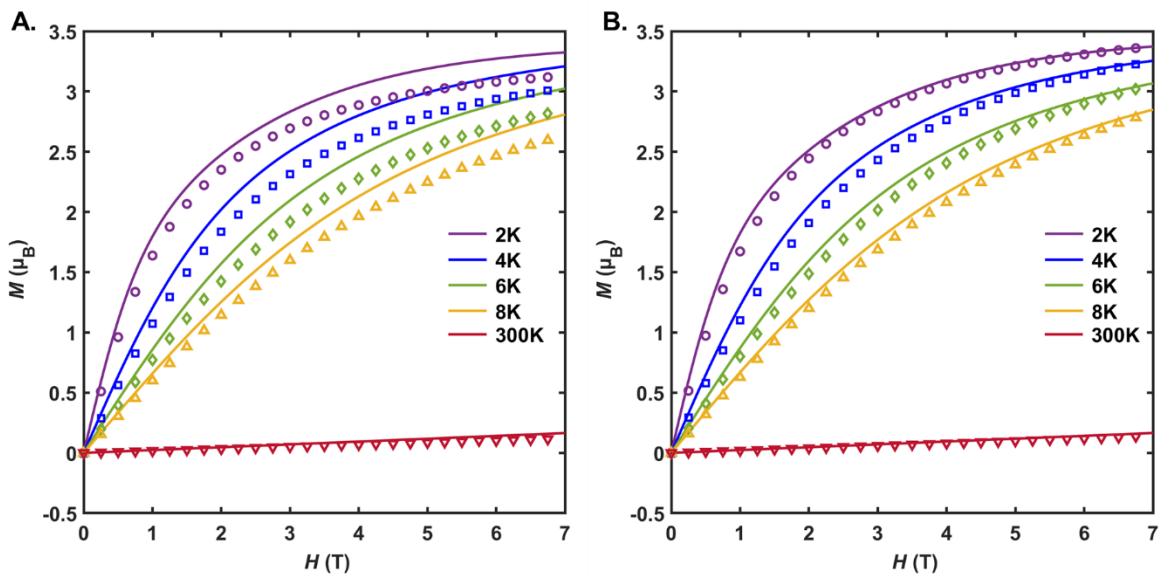

Figure 3.9. *M* vs. *H* plots fitted with PHI of low iron-loaded PDA samples at **(A)** high Tris concentration (pH ~ 9.77, $J = -31$ cm^{-1}, Percent coupled = 31%) and **(B)** low Tris concentration (pH ~ 8.61, $J = -12$ cm^{-1}, Percent coupled = 30%).[68]

Not unlike the high iron loaded samples, these models for these systems require further optimization. Nevertheless, the simulation generated for the low iron loaded sample prepared at low Tris concentrations closely resemble its magnetization behavior, offering strong evidence that the parameters used are close to the actual values of this system.

CHAPTER 4: CONCLUSIONS AND OUTLOOK

4.1 Conclusion

Polydopamine aggregated nanomaterials were prepared and characterized using magnetometry to probe the effects of small alterations in the synthetic parameters. Further corroboration is required, the data offer strong evidence that variations in the buffer concentration significantly affect the coupling strength between metal centers. Furthermore, preliminary data

from a study currently in progress indicate that $\chi_M T$ of the material is greatly influenced by the concentration of iron present in the sample (data not shown), and therefore it is imperative to optimize the quantification methods. Finally, while further work is required for optimization, a workable model for the magnetization data has been developed in which the simulated data closely resembles those of the actual system.

4.2 Forthcoming Work

The results as described in this work show remarkable promise for future investigation of the electronic structure of synthetic melanins *via* magnetometry. The following sections describe proposed studies for the advancement of this work.

4.2.1 Continued Studies of Fe(III)-loaded PDA Materials

Effect of pH on Magnetic Properties

While the concentration of Tris, and effectively its effect on the pH of the synthesis of the nanomaterial, appears to influence the magnetic properties of the samples, no clear conclusions can be drawn at this time. Studies aimed to investigate the effect of various bases and their concentrations on the behavior of magnetically active metal-doped PDA samples are currently underway. The samples described in Section 2.1.6 have been prepared for future magnetic analysis to determine the correlation between coupling strength and base used, if any.

Additionally, because it is unclear whether the difference in coupling strength is due to the pH of the reaction system during polymer synthesis, the amount of Tris buffer used, or a mixture of both, future studies aim to magnetically analyze samples prepared using a non-incorporating base (i.e. phosphate buffer) to determine if pH influences the magnetic behavior of these samples. Additionally, because it is known that Tris buffer is incorporated into the PDA manifold, studies varying pH with this buffer will be carried out as well, in which the amount of Tris used to prepared

the buffer solution remains constant, while the amount of the solvent is varied. The objective of these studies is two-fold: i) preparing samples with a non-incorporating base will probe the effects of only pH on the magnetic behavior of the material. If no change occurs, then it can be assumed that pH is not influential on the coupling strength; ii) however, if a change is observed, then it will be necessary to determine if the incorporation of Tris has an added effect on the magnetism. If pH does affect the coupling strength while the incorporation of Tris does not, then a similar coupling constant should be observed in both experiments at similar pH. If pH does not affect the coupling strength, but the incorporation of Tris does, the difference in coupling constant, *J*, between both experiments should be consistent at each pH. Trends in the effect of both pH and amount of Tris can then be determined by comparing the results of all three studies.

Determining these effects on the magnetic behavior of these materials may be potentially advantageous in tuning the strength of antiferromagnetic coupling and may be purposed for other applications, such as reducing the antiferromagnetic coupling in MRI contrast agents.

4.2.2 Continued Studies of Fe(II)-loaded PDA Materials

Effects of pH on Magnetic Properties

Ideally, these studies will extend to other oxidation states of multivalent metals, namely Fe(II). While the objective is to fabricate a metal-PDA system in which all metal centers are Fe(II), this may prove to be a formidable challenge as Fe(II) is readily oxidized by O_2 in the air, especially in acidic chloride solutions.[69] Additionally, O_2 is required for the oxidation of the catechol group to initiate polymerization and the reaction solution becomes acidic (pH ~2-3) due to the dissociation of HCl in the dopamine salt starting material. To overcome this challenge, Fe(II) can be incorporated into the PDA scaffold using the metal ion exchange strategy in which PDA can be doped with manganese ions in ambient conditions. To prevent oxidation of the Fe^{2+} ions in

solution, the ion exchange will occur under inert atmosphere. It is unknown if the Fe^{2+} ions are oxidized after polymerization, however, this may be probed by comparing the magnetic analyses of samples prepared by aerobic metal ion exchange and samples prepared by anaerobic metal exchange against that of the Fe(III)-PDA samples to determine if there are any notable disparities.

It would also be valuable to optimize the tunability of mixed-valence systems in which the ratio of Fe(II) : Fe(III) can be controlled. Stabilization of all oxidation states of iron would effectively reduce the energy barrier in redox coupling through the delocalization of charge within the PDA network, allowing access to different active sites within the manifold, thereby accessing a plethora of untapped chemistries. Xie *et al*. demonstrated that Fe(II)-PDOPA exhibits peroxidase-esque activity twice as effective than that of Fe(III)-PDOPA *via* Fenton-like chemistry, which could potentially be applied to cancer therapies. However, they did note that the Fe(II)-PDOPA sample may have undergone partial oxidation in which the Fe(II) : Fe(III) ratio is unknown.[70]

4.2.3 Investigation of other Metal-loaded Synthetic Melanin Materials

While methods using Mn(III)-PDA as a template for metal ion exchange have been previously reported, it would be interesting to incorporate other oxidation states of manganese and explore their effects on exchange efficacy. It is currently unknown if the different oxidation states of manganese have any effect on the overall structure of the PDA polymer, even though these different oxidation states are likely to influence how the catechol ligands chelate. Additionally, investigation of other metals that may be beneficial to examine are cobalt, nickel, and copper, which have all been reported to successfully incorporate into the structure of the polymer. For a similar reason discussed in Section 4.2.2, stabilization of the various valences of these metals may

allow access to a variety of chemical activity which have not yet been observed in PDA, offering further insight into the electronic structure of the material.

Likewise, the effect of different starting monomers, such as L-DOPA and 1,8-dihydroxynaphthalene (1,8-DHN), on the magnetic properties of these materials has yet to be explored, especially since the structure, and consequently the polymerization mechanism, of 1,8-DHN would be starkly different from that of DA or DOPA, which are relatively similar in structure. Nevertheless, probing each parameter in the preparation of synthetic melanins would be valuable in thoroughly understand how each variable affects the electronic structure of the material.

4.2.4 Investigation of the Magnetic Properties of Natural Melanins

One purpose of probing the magnetic properties of synthetic melanins is to gain insight and refine future studies of the possible structure and function of natural melanins, since natural and synthetic melanins have been demonstrated to possess several similar properties. It had been previously discussed that the difficulty of isolation and purification of natural melanins is variable. However, with the promising magnetic data shown in synthetic melanins, extending these studies to natural melanins would prove incredibly advantageous in the capability of studying the natural system directly, namely to what extent these materials are capable of sequestering metal ions from their environment. Indeed, further study of the form of natural melanins would prove to be beneficial in understanding, and consequently optimizing, the material's function purposed for myriad future applications.

APPENDIX

A1 Supplementary Information

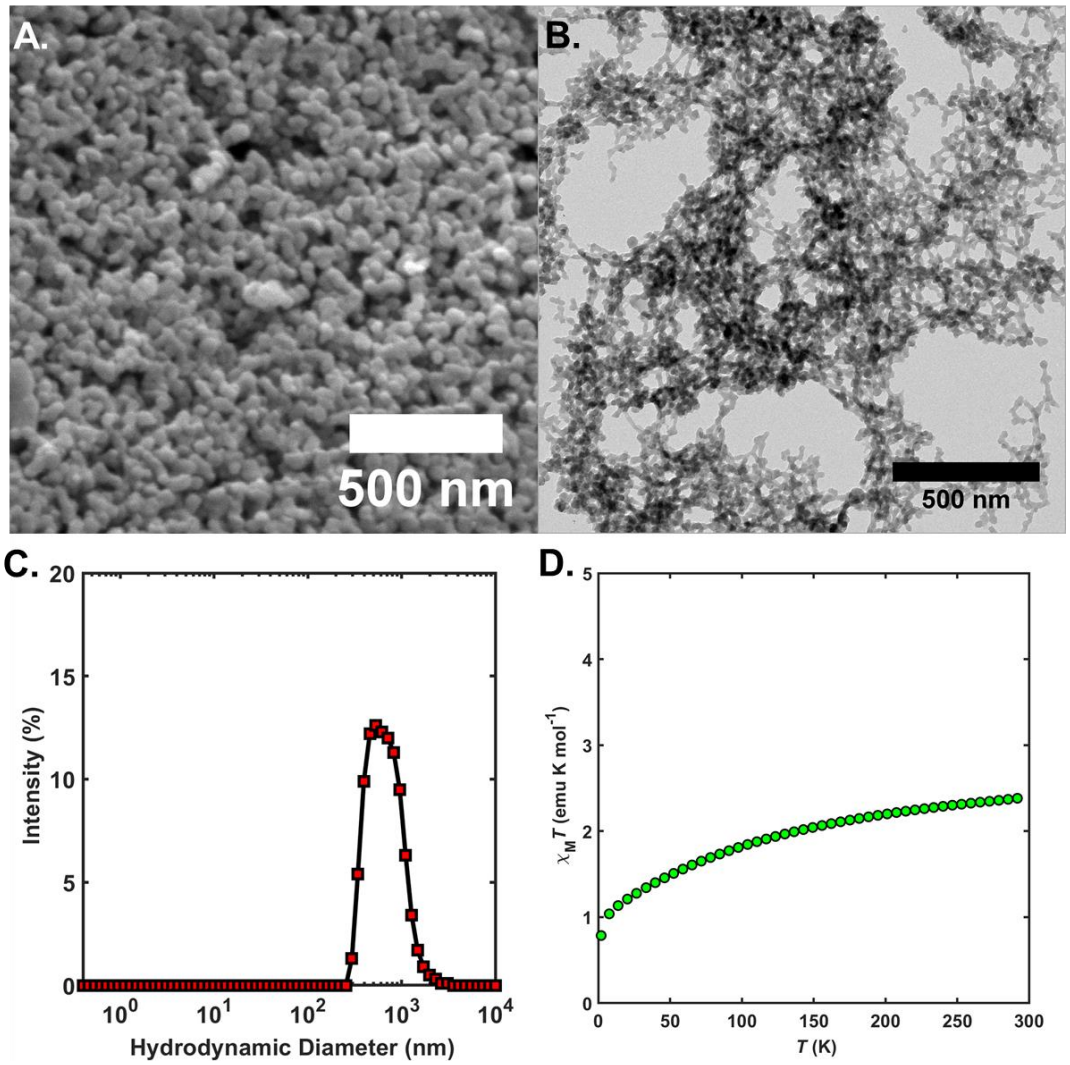

Figure A1. PDA aggregated materials with high concentrations of iron **(A)** SEM image; **(B)** TEM image; **(C)** DLS analysis of the hydrodynamic diameter distribution of Fe(III)-PDA; **(D)** $\chi_M T$ vs. T plot of Fe(III)-PDA with high loadings of iron prepared with Tris concentrations as previously reported.

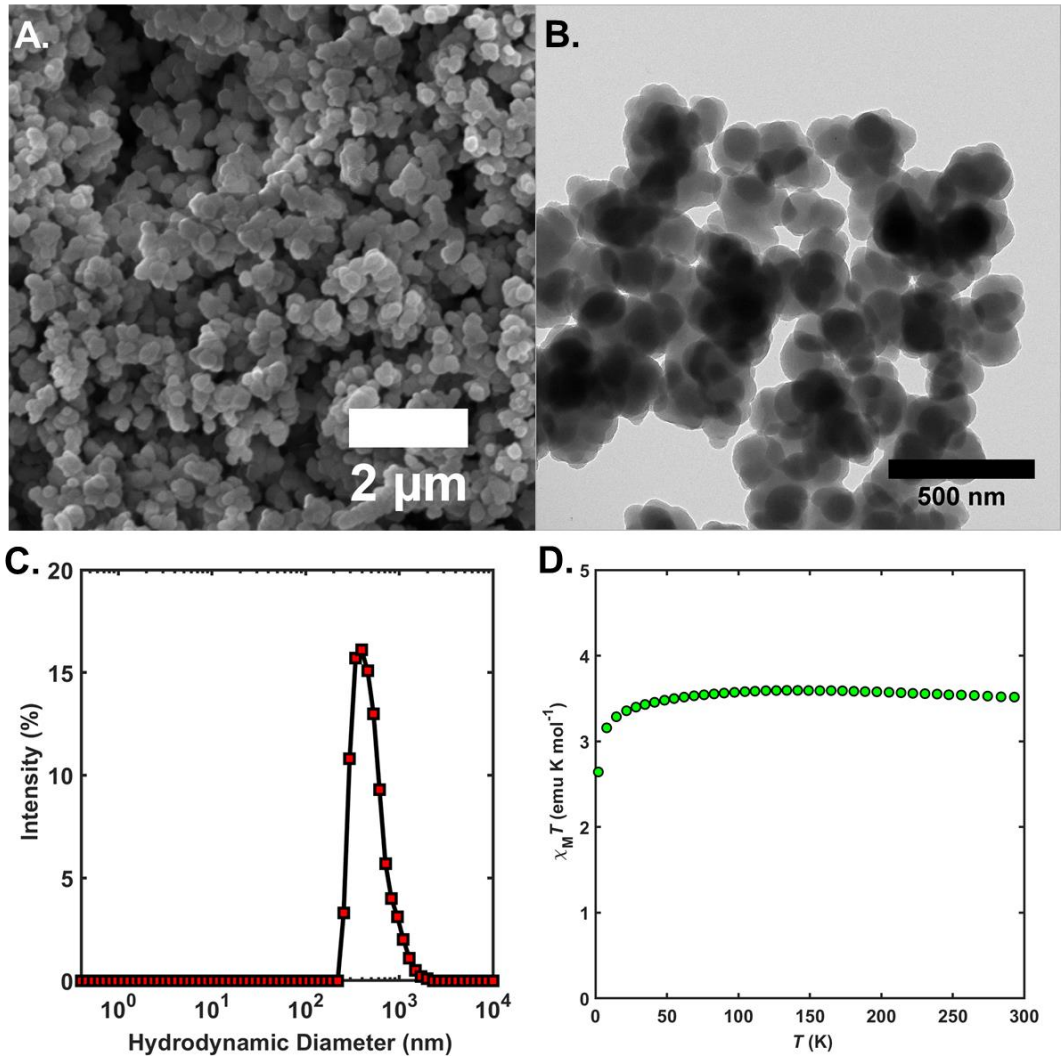

Figure A2. PDA aggregated materials with low concentrations of iron **(A)** SEM image; **(B)** TEM image; **(C)** DLS analysis of the hydrodynamic diameter distribution of Fe(III)-PDA; **(D)** $\chi_M T$ vs. T plot of Fe(III)-PDA with high loadings of iron prepared with Tris concentrations as previously reported.

This thesis is co-authored with Cay, Kristine S., Fong, Hayley A. and Rinehart, Jeffrey D.

The thesis author was the primary author of this work.

REFERENCES

1. Cichorek, M.; Wachulska, M; Stasiewicz, A.; Tymińska, A. 'Skin Melanocytes: Biology and Development'. *Advances in Dermatology and Allergology/Postępy Dermatologii I Alergologii* **2013**, *30* (1), 30–41.

2. Ismael, G. and Solano, F.. 'Bird Integumentary Melanins: Biosynthesis, Forms, Function and Evolution'. *International Journal of Molecular Sciences.* **2016**, *17*(4), 520.

3. Riley, P. A. 'Melanin'. *The International Journal of Biochemistry & Cell Biology*. **1997**, *29*(11), 1235–1239.

4. Watt, A. A. R.; Bothma, J. P.; Meredith, P. 'The Supramolecular Structure of Melanin'. *Soft Matter*. **2009**, *5*(19), 3754–3760.

5. Shosuke, I. 'Optimization of Conditions for Preparing Synthetic Pheomelanin'. *Pigment Cell Research*. **1989**, *2*(1) 53–56.

6. Zecca, L.; D Tampellini, D.; Gerlach, M; Riederer, P; Fariello, R. G.; Sulzer, D. 'Substantia Nigra Neuromelanin: Structure, Synthesis, and Molecular Behaviour'. *Molecular Pathology*. **2001**, *54*(6), 414–418.

7. Westerhof, W. 'The Discovery of the Human Melanocyte'. *Pigment Cell Research*. **2006**, *19*(3), 183–193.

8. d'Ischia, M.; Wakamatsu, K.; Napolitano, A.; Briganti, S.; Garcia-Borron, J.-C.; Kovacs, D.;, Meredith, P.; Pezzella, A.; Picardo, M.; Sarna, T.; Simon, J. D.; Ito, S. 'Melanins and Melanogenesis: Methods, Standards, Protocols'. *Pigment Cell & Melanoma Research.* **2013**, *26*(5), 616–633.

9. Liebscher, J. 'Chemistry of Polydopamine – Scope, Variation, and Limitation'. *European Journal of Organic Chemistry*. **2019**, *31–32* (2019), 4976–4994.

10. Liu, Y.; Ai, K.; Lu, L. 'Polydopamine and Its Derivative Materials: Synthesis and Promising Applications in Energy, Environmental, and Biomedical Fields'. *Chemical Reviews*. **2014**, *114*(9), 5057–5115.

11. d'Ischia, M.; Napolitano, A.; Ball, V.; Chen, C.-T.; Buehler, M. J. 'Polydopamine and Eumelanin: From Structure–Property Relationships to a Unified Tailoring Strategy'. *Accounts of Chemical Research*. **2014**, *47*(12), 3541–3550.

12. Dreyer, D. R.; Miller, D. J.; Freeman, B. D.; Paul, D. R.; Bielawski, C. W. 'Elucidating the Structure of Poly(Dopamine)'. *Langmuir*. **2012**, *28*(15) 6428–6435.

13. Crescenzi, O.; Kroesche, C.; Hoffbauer, W.; Jansen, M.; Napolitano, A.; Prota, G.; Peter, M. G. 'Synthesis of Dopamines Labelled with 13C in the α- or β-Side Chain Position and Their Application to Structural Studies on Melanins by Solid-State NMR Spectroscopy'. *Liebigs Annalen Der Chemie.* **1994**, *1994*(6), 563–567.

14. Jiang, J.-H.; Zhu, L.-P.; Li, X.-L.; Xu, Y.-Y.; Zhu, B.-K.. 'Surface Modification of PE Porous Membranes Based on the Strong Adhesion of Polydopamine and Covalent Immobilization of Heparin'. *Journal of Membrane Science*. **2010**, *364*(1), 194–202.

15. Tse, D. C. S.; McCreery, R. L.; Adams, R. N. 'Potential Oxidative Pathways of Brain Catecholamines'. *Journal of Medicinal Chemistry*. **1976**, *19*(1), 37–40.

16. Patil, A. O.; Pennington, W. T.; Desiraju, G. R.; Curtin, D. Y.; Paul, I. C. 'Recent Studies on the Formation and Properties of Quinhydrone Complexes'. *Molecular Crystals and Liquid Crystals*. **1986**, *134*(1), 279–304.

17. Senoh, S.; Creveling, C. R.; Udenfriend, S.; Witkop, B. 'Chemical, Enzymatic and Metabolic Studies on the Mechanism of Oxidation of Dopamine'. *Journal of the American Chemical Society*.**1959**, *81*(23), 6236–6240.

18. Cataldo, F. 'On the Structure of Macromolecules Obtained by Oxidative Polymerization of Polyhydroxyphenols and Quinones'. *Polymer International.* **1998**, *46*(4), 263–268.

19. Liebscher, J.; Mrówczyński, R.; Scheidt, H. A.; Filip, C.; Hădade, N. D.; Turcu, R.; Bende, A.; Beck, S. 'Structure of Polydopamine: A Never-Ending Story?' *Langmuir*. **2013**, *29*(33), 10539–10548.

20. Haeshin, L.; Dellatore, S. M.; Miller, W. M.; Messersmith, P. B. 'Mussel-Inspired Surface Chemistry for Multifunctional Coatings'. *Science*. **2007**, *318*(5849), 426–430.

21. Shalev, T.; Gopin, A.; Bauer, M.; Stark, R. W.; Rahimipour, S. 'Non-Leaching Antimicrobial Surfaces through Polydopamine Bio-Inspired Coating of Quaternary Ammonium Salts or an Ultrashort Antimicrobial Lipopeptide'. *Journal of Materials Chemistry*. **2012**, *22*(5), 2026–2032.

22. Della Vecchia, N. F.; Luchini, A.; Napolitano, A.; D'Errico, G.; Vitiello, G.; Szekely, N.; Marco d'Ischia; Paduano, L. 'Tris Buffer Modulates Polydopamine Growth, Aggregation, and Paramagnetic Properties'. *Langmuir*. **2014**, *30*(32), 9811–9118.

23. Arzillo, M.; Mangiapia, G.; Pezzella, A.; Heenan, R. K.; Radulescu, A.; Paduano, L.; d'Ischia, M. 'Eumelanin Buildup on the Nanoscale: Aggregate Growth/Assembly and Visible Absorption Development in Biomimetic 5,6-Dihydroxyindole Polymerization.' *Biomacromolecules.* **2012**, *13*(8), 2379–2390.

24. Alfieri, M. L.; Micillo, R.; Panzella, L.; Crescenzi, O.; Oscurato, S. L.; Maddalena, P.; Napolitano, A.; Ball, V.; d'Ischia, M. 'Structural Basis of Polydopamine Film Formation:

Probing 5,6-Dihydroxyindole-Based Eumelanin Type Units and the Porphyrin Issue'. *ACS Applied Materials & Interfaces.* **2018**, *10*(9), 7670–7680.

25. Delparastan, P.; Malollari, K. G.; Lee, H.; Messersmith, P. B. 'Direct Evidence for the Polymeric Nature of Polydopamine'. *Angewandte Chemie.* **2019**, *131*(4), 1089–1094.

26. Yang, J.; Cohen Stuart, M. A.; Kamperman, M.. 'Jack of All Trades: Versatile Catechol Crosslinking Mechanisms'. *Chemical Society Reviews.* **2014**, *43*, 8271-8298.

27. Ito, S. and Wakamatsu, K. 'Chemistry of Mixed Melanogenesis—Pivotal Roles of Dopaquinone†'. *Photochemistry and Photobiology*. **2008**, *84*(3), 582–592.

28. Cooksey, C. J.; Garratt, P. J.; Land, E. J.; Pavel, S.; Ramsden, C. A.; Riley, P. A.; and Smit, N. P. M. 'Evidence of the Indirect Formation of the Catecholic Intermediate Substrate Responsible for the Autoactivation Kinetics of Tyrosinase'. *Journal of Biological Chemistry*.**1997**, *272*(42), 26226–26235.

29. Raper, H. St. 'The Tyrosinase-Tyrosine Reaction'. *Biochemical Journal*. **1927**, *21*(1), 89–96.

30. Mason, H. S. and Wright, C. I. 'The chemistry of melanin. V. Mechanism of the oxidation of dihydroxyphenylalanine by tyrosinase'. *Journal of Biological Chemistry.* **1949**, *180*, 235-247.

31. Raper, H. S. 'Some Problems of Tyrosine Metabolism'. *Journal of the Chemical Society (Resumed)*, **1938**, 125.

32. Hong, Seonki, Yun Suk Na, Sunghwan Choi, In Taek Song, Woo Youn Kim, and Haeshin Lee. 'Non-Covalent Self-Assembly and Covalent Polymerization Co-Contribute to Polydopamine Formation'. *Advanced Functional Materials*. **2012**, *22*(22), 4711–4717.

33. Bittner, S. 'When Quinones Meet Amino Acids: Chemical, Physical and Biological Consequences'. *Amino Acids*. **2006**, *30*(3), 205–224.

34. Burzio, L. A. and Waite, J. H. 'Cross-Linking in Adhesive Quinoproteins: Studies with Model Decapeptides'. *Biochemistry*. **2000**, *39*(36), 11147–11153.

35. McDowell, L. M.; Burzio, L. A.; Waite, J. H.; Schaefer, J. 'Rotational Echo Double Resonance Detection of Cross-Links Formed in Mussel Byssus under High-Flow Stress'. *Journal of Biological Chemistry*. **1999**, *274*(29), 20293–20295.

36. Avdeef, A.; Sofen, S. R.; Bregante, T. L.; Raymond, K. N. 'Coordination Chemistry of Microbial Iron Transport Compounds. 9. Stability Constants for Catechol Models of Enterobactin'. *Journal of the American Chemical Society*. **1978**, *100*(17), 5362–5370.

37. Holten-Andersen, N.; Harrington, M. J.; Birkedal, H.; Lee, B. P.; Messersmith, P. B.; Lee, K. Y. C.; Waite, J. H. 'PH-Induced Metal-Ligand Cross-Links Inspired by Mussel Yield Self-Healing Polymer Networks with near-Covalent Elastic Moduli'. *Proceedings of the National Academy of Sciences*. **2011**, *108*(7), 2651.

38. Zeng, H.; Hwang, D. S.; Israelachvili, J. N.; Waite, J. H. 'Strong Reversible Fe3+-Mediated Bridging between Dopa-Containing Protein Films in Water'. *Proceedings of the National Academy of Sciences.* **2010**, *107*, 12850.

39. Yu, F.; Chen, S.; Chen, Y.; Li, H.; Yang, L.; Chen, Y.; Yin, Y. 'Experimental and Theoretical Analysis of Polymerization Reaction Process on the Polydopamine Membranes and Its Corrosion Protection Properties for 304 Stainless Steel'. *Journal of Molecular Structure*. **2010**, *982*(1), 152–161.

40. Sun, Daniel T., Li Peng, Washington S. Reeder, Seyed Mohamad Moosavi, Davide Tiana, David K. Britt, Emad Oveisi, and Wendy L. Queen. 'Rapid, Selective Heavy Metal Removal from Water by a Metal–Organic Framework/Polydopamine Composite'. *ACS Central Science*. **2018**, *4*(3), 349–356.

41. Powell, H. K. J., and M. C. Taylor. 'Interactions of Iron(II) and Iron(III) with Gallic Acid and Its Homologues: A Potentiometric and Spectrophotometric Study'. *Australian Journal of Chemistry*. **1982**, *35*(4), 739–756.

42. Monahan, J. and Wilker, J. J. 'Specificity of Metal Ion Cross-Linking in Marine Mussel Adhesives'. *Chemical Communications*. **2003**, *14*, 1672–1673.

43. Wilker, J. J. 'Marine Bioinorganic Materials: Mussels Pumping Iron'. *Current Opinion in Chemical Biology*, Biocatalysis and Biotransformation/Bioinorganic Chemistry. **2010**, *14*(2), 276–283.

44. Li, Yiwen, Yijun Xie, Zhao Wang, Nanzhi Zang, Fabio Carniato, Yuran Huang, Christopher M. Andolina, et al. 'Structure and Function of Iron-Loaded Synthetic Melanin'. *ACS Nano*. **2016**, *10*(11), 10186–10194.

45. Wang, Z.; Xie, Y.; Li, Y.; Huang, Y.; Parent, L. R.; Ditri, T.; Zang, N.; Rinehart, J. D.; Gianneschi, N. C. 'Tunable, Metal-Loaded Polydopamine Nanoparticles Analyzed by Magnetometry'. *Chemistry of Materials*, **2017**, *29*(19); 8195–8201.

46. Lee, Haeshin, Norbert F. Scherer, and Phillip B. Messersmith. 'Single-Molecule Mechanics of Mussel Adhesion'. *Proceedings of the National Academy of Sciences*. **2006**, *103*(35), 12999–13003.

47. Ooka, A. A. and Garrell, R. L. 'Surface-Enhanced Raman Spectroscopy of DOPA-Containing Peptides Related to Adhesive Protein of Marine Mussel, Mytilus Edulis'. *Biopolymers*. **2000**, *57*(2), 92–102.

48. Lee, B. P.; Dalsin, J. L.; Messersmith, P. B. 'Synthesis and Gelation of DOPA-Modified Poly(Ethylene Glycol) Hydrogels'. *Biomacromolecules*. **2002**, *3*(5), 1038–1047.

49. Lee, B. P.; Chao, C.-Y.; F.; Nunalee, N.; Motan, E.; Shull, K. R.; Messersmith, P. B. 'Rapid Gel Formation and Adhesion in Photocurable and Biodegradable Block Copolymers with High DOPA Content'. *Macromolecules*. **2006**, *39*(5), 1740–1748.

50. Kim, B. H.; Lee, D. H.; Kim, J. Y.; Shin, D. O.; Jeong, H. Y.; Hong, S.; Yun, J. M.; Koo, C. M.; Lee, H; Kim, S. O. 'Mussel-Inspired Block Copolymer Lithography for Low Surface Energy Materials of Teflon, Graphene, and Gold'. *Advanced Materials*. **2011**, *23*(47), 5618–5622.

51. Cheng, C.; Nie, S.; Li, S.; Peng, H.; Yang, H.; Ma, L.; Sun, S.; Zhao, C. 'Biopolymer Functionalized Reduced Graphene Oxide with Enhanced Biocompatibility via Mussel Inspired Coatings/Anchors'. *Journal of Materials Chemistry B*. **2013**, *1*(3), 265–275.

52. Zhu, Y.; Xin, N.; Qiao, Z.; Chen, S.; Zeng, L.; Zhang, Y.; Wei, D.; Sun, J.; Fan, H. 'Novel Tumor-Microenvironment-Based Sequential Catalytic Therapy by Fe(II)-Engineered Polydopamine Nanoparticles'. *ACS Applied Materials & Interfaces*. **2019**, *11*(46), 43018–43030.

53. Wang, Z.; Carniato, F.; Xie, Y.; Huang, Y.; Li, Y.; He, S.; Zang, N.; Rinehart, J. D.; Botta, M.; and Gianneschi, N. C. 'High Relaxivity Gadolinium-Polydopamine Nanoparticles'. *Small*. **2017**, *13*(43), 1701830.

54. Xie, Y.; Wang, J.; Wang, Z.; Krug, K. A.; Rinehart, J. D. 'Perfluorocarbon-Loaded Polydopamine Nanoparticles as Ultrasound Contrast Agents'. *Nanoscale*. **2018**, *10*(26), 12813–12819.

55. Xie, Y.; Wang, J.; Wang, J.; Hu, Z.; Hariri, A.; Tu, N.; Krug, K. A.; Burkart, M. D.; Gianneschi, N. C.; Jokerst, J. V.; Rinehart, J. D. 'Tuning the Ultrasonic and Photoacoustic Response of Polydopamine-Stabilized Perfluorocarbon Contrast Agents'. *Journal of Materials Chemistry B*. **2019**, *7*(31), 4833–4842.

56. Ryou, M.-H.; Lee, Y. M.; Park, J.-K.; Choi, J. W. 'Mussel-Inspired Polydopamine-Treated Polyethylene Separators for High-Power Li-Ion Batteries'. *Advanced Materials*. **2011**, *23*(27), 3066–3070.

57. Ryou, Myung-Hyun, Dong Jin Lee, Je-Nam Lee, Yong Min Lee, Jung-Ki Park, and Jang Wook Choi. 'Excellent Cycle Life of Lithium-Metal Anodes in Lithium-Ion Batteries with Mussel-Inspired Polydopamine-Coated Separators'. *Advanced Energy Materials*. **2012**, *2*(6), 645–650.

58. Liu, Nian, Hui Wu, Matthew T. McDowell, Yan Yao, Chongmin Wang, and Yi Cui. 'A Yolk-Shell Design for Stabilized and Scalable Li-Ion Battery Alloy Anodes'. *Nano Letters*. **2012**, *12*(6), 3315–3321.

59. Kang, S. M.; Ryou, M.-H.; Choi, J. W.; Lee, H. 'Mussel- and Diatom-Inspired Silica Coating on Separators Yields Improved Power and Safety in Li-Ion Batteries'. *Chemistry of Materials*. **2012**, *24*(17), 3481–3485.

60. Jiang, H.; Yang, L.; Li, C.; Yan, C.; Lee, P. S.; Ma, J. 'High–Rate Electrochemical Capacitors from Highly Graphitic Carbon–Tipped Manganese Oxide/Mesoporous Carbon/Manganese Oxide Hybrid Nanowires'. *Energy & Environmental Science*. **2011**, *4*(5), 1813–1819.

61. Farnad, N.; Farhadi, K.; Voelcker, N. H. 'Polydopamine Nanoparticles as a New and Highly Selective Biosorbent for the Removal of Copper (II) Ions from Aqueous Solutions'. *Water, Air, & Soil Pollution*. **2012**, *223*(6), 3535–3544.

62. Hongcai, Yimin Sun, Jiajing Zhou, Rong Xu, and Hongwei Duan. 'Mussel-Inspired Synthesis of Polydopamine-Functionalized Graphene Hydrogel as Reusable Adsorbents for Water Purification'. *ACS Applied Materials & Interfaces*. **2013**, *5*(2), 425–432.

63. Huang, S.; Yang, L.; Liu, M.; Phua, S. L.; Yee, W. A.; Liu, W.; Zhou, R.; Lu, X. 'Complexes of Polydopamine-Modified Clay and Ferric Ions as the Framework for Pollutant-Absorbing Supramolecular Hydrogels'. *Langmuir*. **2013**, *29*(4), 1238–1244.

64. Sun, G.; Chung, T.-S.; Jeyaseelan, K.; Armugam, A. 'Stabilization and Immobilization of Aquaporin Reconstituted Lipid Vesicles for Water Purification'. *Colloids and Surfaces B: Biointerfaces*. **2013**, *102*, 466–471.

65. Han, G.; Zhang, S.; Li, X.; Widjojo, N.; Chung, T.-S. 'Thin Film Composite Forward Osmosis Membranes Based on Polydopamine Modified Polysulfone Substrates with Enhancements in Both Water Flux and Salt Rejection'. *Chemical Engineering Science*. 2012, *80*, 219–231.

66. Ju, K.-Y.; Lee, Y.; Lee, S.; Park, S. B.; Lee, J.-K. 'Bioinspired Polymerisation of Dopamine to Generate Melanin-like Nanoparticles Having an Excellent Free-Radical-Scavenging Property'. *Biomacromolecules*, **2011**, *12*, 625-623.

67. Kahn, O. *Molecular Magnetism*; VCH Publishers, Inc.: New York, 1942.

68. Chilton, N. F., Anderson, R. P.; Turner, L. D.; Soncini, A.; Murray, K. S. 'PHI: A Powerful New Program for the Analysis of Anisotropic Monomeric and Exchange-Coupled Polynuclear d- and f-Block Complexes'. *Journal of Computational Chemistry*. **2013**, *34*(13), 1164–1175.

69. Akilan, Chandrika, and Michael J Nicol. 'Kinetics of the Oxidation of Iron(II) by Oxygen and Hydrogen Peroxide in Concentrated Chloride Solutions – A Re-Evaluation and Comparison with the Oxidation of Copper(I)'. *Hydrometallurgy*. **2016**, *166*, 123–129.

70. Xie, Y.; Krug, K.; **Cay, K. S.**; Kalaj, M.; Collin-McCallum, N.; Siwicka, Z.; Wang, Z.; Gianneschi, N.; Burkart, M.; Rinehart, J. D. “Peroxidase-like reactivity at iron-chelation sites in a mesoporous synthetic melanin.” **Under review**.